

# Probing scalar induced gravitational waves with PTA and LISA: The Importance of third order correction

Zhe Chang,<sup>a,b</sup> Yu-Ting Kuang,<sup>a,b,1</sup> Di Wu,<sup>a,b</sup> Jing-Zhi Zhou<sup>a,b</sup>

<sup>a</sup>Institute of High Energy Physics, Chinese Academy of Sciences, Beijing 100049, China

<sup>b</sup>University of Chinese Academy of Sciences, Beijing 100049, China

E-mail: [changz@ihep.ac.cn](mailto:changz@ihep.ac.cn), [kuangyt@ihep.ac.cn](mailto:kuangyt@ihep.ac.cn), [wudi@ihep.ac.cn](mailto:wudi@ihep.ac.cn),  
[zhoujingzhi@ihep.ac.cn](mailto:zhoujingzhi@ihep.ac.cn)

**Abstract.** We revisit the calculation of third order scalar induced gravitational waves (SIGWs) and extend it from a monochromatic primordial power spectrum to a more general log-normal one. We investigate the impact of third order SIGWs on signal-to-noise ratio (SNR) of Laser Interferometer Space Antenna (LISA) and pulsar timing array (PTA) observations, and find that third order SIGWs significantly contribute to the total energy density spectrum of gravitational waves (GWs) in high-frequency region. For a primordial power spectrum amplitude of  $A_\zeta = 10^{-2} \sim 10^{-1}$ , the effects of third order SIGWs lead to a 40% to 400% increase in the SNR for LISA. Additionally, our PTA data analysis reveals that third order SIGWs diminish both the amplitude  $A_\zeta$  and the peak frequency  $f_*$  of the primordial power spectrum.

---

<sup>1</sup>Corresponding author.

---

## Contents

<b>1</b>	<b>Introduction</b>	<b>1</b>
<b>2</b>	<b>Second and third order scalar induced gravitational waves (SIGWs)</b>	<b>2</b>
2.1	Equations of motion	3
2.2	Power spectra of scalar induced gravitational waves (SIGWs)	5
<b>3</b>	<b>Energy density spectrum with lognormal primordial power spectrum</b>	<b>6</b>
<b>4</b>	<b>Detection of scalar induced gravitational waves (SIGWs)</b>	<b>10</b>
4.1	Signal-to-noise ratio of LISA	10
4.2	PTA observations	11
<b>5</b>	<b>Conclusion and discussion</b>	<b>12</b>
<b>A</b>	<b>Polarization tensors</b>	<b>15</b>
<b>B</b>	<b>Six-point function</b>	<b>16</b>
<b>C</b>	<b>Two-loop diagrams of third order scalar induced gravitational waves (SIGWs)</b>	<b>16</b>

---

## 1 Introduction

The study of stochastic gravitational wave background (SGWB) has been ongoing for many years, and various origins have been proposed, including cosmological phase transition [1, 2], cosmic strings, domain walls [3–5], supermassive black hole binary (SMBHB) [6, 7], and scalar induced gravitational waves (SIGWs) [8, 9]. The latest observations by NANOGrav [10–12], EPTA [13–18], PPTA [19–21], and CPTA [22] have uncovered evidence of the existence of SGWB and provided greater insight into the origins of the SGWB. Extensive research into the origin of SGWB has been conducted through PTA data [23–33]. With the Bayes factor, it was found that SIGWs is a possible candidate for the SGWBs observed by PTA [12]. This paper focuses on the SGWBs dominated by SIGWs.

During the inflation, the primordial cosmological perturbations were generated by the quantum fluctuations. Based on helicity decomposition of metric perturbations, primordial perturbations can be decomposed as scalar, vector, and tensor perturbations. Since the primordial vector perturbation decays very fast [34], it has little influence on the evolution of the Universe. Observations of the cosmic microwave background (CMB) give very tight limits on scalar and tensor perturbations at large scales, while there are almost no constraints on these perturbations at small scales [35]. Thus, a sufficiently large energy density spectrum of SIGWs can be obtained from the power spectra of larger primordial perturbations on the small scales. In addition, unlike CMB, which can only provide the physics imprinted on its last-scattering surface, SIGWs can carry information with higher redshift. More precisely, the pulsar timing array (PTA), as well as the future observations by Laser Interferometer Space Antenna (LISA) and Taiji of the SGWBs, emerge as probes for primordial perturbations generated during inflation. Consequently, we can constrain the parameters of the inflation models in terms of the observation of SIGWs.

The SIGWs have been studied for many years as a prediction of cosmological perturbation theory. There are lots of research related to second order SIGWs, including primordial non-Gaussianity [36–38], the relationship with primordial black holes (PBHs) [39, 40], gauge issue [41–44], damping effect [45, 46] and so on. For the third order SIGWs, Ref. [47] partly considered the third order effects of SIGWs which are induced by first order scalar perturbation directly. In

Refs. [48, 49], we considered all kinds of source terms and investigated the third order SIGWs systematically. In Refs. [50], the impact of third order SIGWs on CMB, Big Bang Nucleosynthesis (BBN), and PTA observations were investigated. However, in previous research on third order SIGWs, the focus was on monochromatic primordial power spectra characterized by infinitesimal width and infinitely high peak. Under these conditions, third order SIGWs have a significant impact on the energy density spectrum in the high-frequency region. Notably, when  $A_\zeta \sim 10^{-2}$ , third order SIGWs exhibit energy density levels comparable to second order SIGWs. In this paper, we revisit the topic of third order SIGWs. We explore a more realistic log-normal primordial power spectrum and systematically analyze the contributions of various source terms to the energy density spectrum of third order SIGWs. We find that the substantial contribution of the third order SIGWs in the high-frequency region is not solely due to the special nature of monochromatic power spectra, this contribution also persists for more general log-normal primordial power spectra.

This paper is organized as follows. In Sec. 2, we review the second and third order SIGWs. In Sec. 3 we investigate the energy density spectra of third order SIGWs for the log-normal primordial power spectra. In Sec. 4, we perform Bayesian analysis by combining PTA observational data and investigate the impact of third order SIGWs on the signal-to-noise ratio (SNR) of LISA. Finally, we summarize our results and give some discussions in Sec. 5.

## 2 Second and third order SIGWs

In this section, we briefly review the main results of second and third order SIGWs during the radiation-dominated (RD) era. The perturbed metric in the flat Friedmann-Lemaitre-Robertson-Walker (FLRW) spacetime with Newtonian gauge is given by

$$ds^2 = a^2(\eta) \left[ - \left( 1 + 2\phi^{(1)} + \phi^{(2)} \right) d\eta^2 + V_i^{(2)} d\eta dx^i + \left( \left( 1 - 2\psi^{(1)} - \psi^{(2)} \right) \delta_{ij} + \frac{1}{2} h_{ij}^{(2)} + \frac{1}{6} h_{ij}^{(3)} \right) dx^i dx^j \right], \quad (2.1)$$

where  $\eta$  is the conformal time.  $\phi^{(n)}$  and  $\psi^{(n)}$  ( $n = 1, 2$ ) are first order and second order scalar perturbations.  $h_{ij}^{(n)}$  ( $n = 2, 3$ ) are second order and third order tensor perturbations.  $V_i^{(2)}$  is second order vector perturbation. Here, we have neglected the first order vector and tensor perturbations. The total contributions of SIGWs up to third order can be written as

$$h_{ij}(\mathbf{x}, \eta) = \frac{1}{2} h_{ij}^{(2)}(\mathbf{x}, \eta) + \frac{1}{6} h_{ij}^{(3)}(\mathbf{x}, \eta), \quad (2.2)$$

where  $h_{ij}^{(2)}(\mathbf{x}, \eta)$  and  $h_{ij}^{(3)}(\mathbf{x}, \eta)$  are known as second and third order SIGWs respectively. The Fourier components of  $h_{ij}^{(n)}(\mathbf{x}, \eta)$  ( $n = 2, 3$ ) in terms of the polarization tensors  $\varepsilon_{ij}^\lambda(\mathbf{k})$  ( $\lambda = +, \times$ ) are defined as

$$h_{ij}^{(n)}(\mathbf{x}, \eta) = \int \frac{d^3k}{(2\pi)^{3/2}} e^{i\mathbf{k}\cdot\mathbf{x}} \left( h_{\mathbf{k}}^{+, (n)}(\eta) \varepsilon_{ij}^+(\mathbf{k}) + h_{\mathbf{k}}^{\times, (n)}(\eta) \varepsilon_{ij}^\times(\mathbf{k}) \right), \quad (n = 2, 3). \quad (2.3)$$

The explicit expressions of the polarization tensors  $\varepsilon_{ij}^\lambda(\mathbf{k})$  ( $\lambda = +, \times$ ) are given in Appendix. A. In Sec. 2.1, we will present three second order perturbations that are induced by first order scalar perturbation. We will then discuss third order gravitational waves that are induced by all lower order perturbations. The power spectra of second and third order SIGWs and corresponding loop diagrams will be investigated in Sec. 2.2.

## 2.1 Equations of motion

To calculate the second and third order SIGWs in Eq. (2.3), we need to solve the cosmological perturbation equation order by order. The equations of motion of first order scalar perturbations can be written as [51]

$$\begin{aligned} 3\psi^{(1)''}(\mathbf{x}, \eta) - \Delta\psi^{(1)}(\mathbf{x}, \eta) + 3\mathcal{H}\left(\phi^{(1)'}(\mathbf{x}, \eta) + 3\psi^{(1)'}(\mathbf{x}, \eta)\right) &= 0, \\ \psi^{(1)}(\mathbf{x}, \eta) - \phi^{(1)}(\mathbf{x}, \eta) &= 0, \end{aligned} \quad (2.4)$$

where the prime denotes the derivative with respect to the conformal time  $\eta$ .  $\mathcal{H} = a'/a$  is the conformal Hubble parameter. By solving Eq. (2.4) during the RD era ( $\mathcal{H} = 1/\eta$ ,  $\omega = 1/3$ , and  $c_s^2 = 1/3$ ), we obtain the first order scalar perturbations in momentum space:  $\phi(\mathbf{k}, \eta) = \psi(\mathbf{k}, \eta) = \frac{2}{3}\zeta_{\mathbf{k}}T_\phi(|\mathbf{k}|\eta)$ , where  $\zeta_{\mathbf{k}}$  is the primordial curvature perturbation. The transfer function  $T_\phi(|\mathbf{k}|\eta)$  of first order scalar perturbation is given by  $T_\phi(|\mathbf{k}|\eta) = \frac{9}{(|\mathbf{k}|\eta)^2} \left( \frac{\sqrt{3}}{|\mathbf{k}|\eta} \sin\left(\frac{|\mathbf{k}|\eta}{\sqrt{3}}\right) - \cos\left(\frac{|\mathbf{k}|\eta}{\sqrt{3}}\right) \right)$  [51].

The equations of motion of three kinds of second order cosmological perturbations are given by [9, 51, 52]

$$\psi^{(2)}(\mathbf{x}, \eta) - \phi^{(2)}(\mathbf{x}, \eta) = -2\Delta^{-1} \left( \partial^r \Delta^{-1} \partial^s - \frac{1}{2} \mathcal{T}^{rs} \right) \mathcal{S}_{rs}^{(2)}(\mathbf{x}, \eta), \quad (2.5)$$

$$\begin{aligned} \psi^{(2)''}(\mathbf{x}, \eta) + 3\mathcal{H}\psi^{(2)'}(\mathbf{x}, \eta) - \frac{5}{6}\Delta\psi^{(2)}(\mathbf{x}, \eta) + \mathcal{H}\phi^{(2)'}(\mathbf{x}, \eta) + \frac{1}{2}\Delta\phi^{(2)}(\mathbf{x}, \eta) \\ = -\frac{1}{2}\mathcal{T}^{rs}\mathcal{S}_{rs}^{(2)}(\mathbf{x}, \eta), \end{aligned} \quad (2.6)$$

$$V_l^{(2)'}(\mathbf{x}, \eta) + 2\mathcal{H}V_l^{(2)}(\mathbf{x}, \eta) = 4\Delta^{-1}\mathcal{T}_l^r\partial^s\mathcal{S}_{rs}^{(2)}(\mathbf{x}, \eta), \quad (2.7)$$

$$h_{lm}^{(2)''}(\mathbf{x}, \eta) + 2\mathcal{H}h_{lm}^{(2)'}(\mathbf{x}, \eta) - \Delta h_{lm}^{(2)}(\mathbf{x}, \eta) = -4\Lambda_{lm}^{rs}\mathcal{S}_{rs}^{(2)}(\mathbf{x}, \eta), \quad (2.8)$$

where  $\Lambda_{rs}^{lm} = \mathcal{T}_r^l\mathcal{T}_s^m - \frac{1}{2}\mathcal{T}_{rs}\mathcal{T}^{lm}$  is the transverse and traceless operator, and  $\mathcal{T}_r^l$  is defined as  $\mathcal{T}_r^l = \delta_r^l - \partial^l\Delta^{-1}\partial_r$ . The source term in Eq. (2.5)–Eq. (2.8) is given by [53]

$$\begin{aligned} \mathcal{S}_{rs}^{(2)}(\mathbf{x}, \eta) &= \partial_r\phi^{(1)}\partial_s\phi^{(1)} + 4\phi^{(1)}\partial_r\partial_s\phi^{(1)} - \frac{1}{\mathcal{H}} \left( \partial_r\phi^{(1)'}\partial_s\phi^{(1)} + \partial_r\phi^{(1)}\partial_s\phi^{(1)'} \right) \\ &\quad - \frac{1}{\mathcal{H}^2}\partial_r\phi^{(1)'}\partial_s\phi^{(1)'} - \delta_{ij} \left( \frac{11}{3}\partial_k\phi^{(1)}\partial^k\phi^{(1)} + 24\mathcal{H}\phi^{(1)}\phi^{(1)'} + \frac{16}{3}\phi^{(1)}\Delta\phi^{(1)} \right. \\ &\quad \left. - \frac{2}{3\mathcal{H}}\partial_k\phi^{(1)'}\partial^k\phi^{(1)} + 2\left(\phi^{(1)'}\right)^2 + 4\phi^{(1)}\phi^{(1)''} - \frac{1}{3\mathcal{H}^2}\partial_k\phi^{(1)'}\partial^k\phi^{(1)'} \right). \end{aligned} \quad (2.9)$$

Eq. (2.5)–Eq. (2.6) and Eq. (2.7) represent the equations of motion of second order scalar induced scalar and vector perturbations respectively. The equation of motion of second order SIGWs is given in Eq. (2.8). By solving Eq. (2.5)–Eq. (2.8), we obtain the second order perturbations in momentum space

$$\psi^{(2)}(\mathbf{k}, \eta) = \int \frac{d^3q}{(2\pi)^{3/2}} I_\psi^{(2)}(|\mathbf{k}-\mathbf{p}|, |\mathbf{p}|, \eta) \zeta_{\mathbf{k}-\mathbf{p}} \zeta_{\mathbf{p}}, \quad (2.10)$$

$$\phi^{(2)}(\mathbf{k}, \eta) = \int \frac{d^3q}{(2\pi)^{3/2}} I_\phi^{(2)}(|\mathbf{k}-\mathbf{p}|, |\mathbf{p}|, \eta) \zeta_{\mathbf{k}-\mathbf{p}} \zeta_{\mathbf{p}}, \quad (2.11)$$

$$V^{\lambda,(2)}(\mathbf{k}, \eta) = \int \frac{d^3p}{(2\pi)^{3/2}} \frac{ik^s e^{\lambda,r}(\mathbf{k})}{k^2} p_r p_s I_V^{(2)}(|\mathbf{k}-\mathbf{p}|, |\mathbf{p}|, \eta) \zeta_{\mathbf{k}-\mathbf{p}} \zeta_{\mathbf{p}}, \quad (2.12)$$

$$h^{\lambda,(2)}(\mathbf{k}, \eta) = \int \frac{d^3p}{(2\pi)^{3/2}} \varepsilon^{\lambda,lm}(\mathbf{k}) p_l p_m I_h^{(2)}(|\mathbf{k}-\mathbf{p}|, |\mathbf{p}|, \eta) \zeta_{\mathbf{k}-\mathbf{p}} \zeta_{\mathbf{p}}, \quad (2.13)$$

where  $I_i^{(2)}$  ( $i = \phi, \psi, V, h$ ) are second order kernel functions. The analytical expressions of second order kernel functions can be found in Refs. [48].

After calculating all first order and second order perturbations, we can systematically study the third order SIGWs. The equation of motion of third order SIGWs is as follows

$$h_{ij}^{(3)''}(\mathbf{x}, \eta) + 2\mathcal{H}h_{ij}^{(3)'}(\mathbf{x}, \eta) - \Delta h_{ij}^{(3)}(\mathbf{x}, \eta) = -12\Lambda_{ij}^{lm} \mathcal{S}_{lm}^{(3)}(\mathbf{x}, \eta), \quad (2.14)$$

where the third order source term  $\mathcal{S}_{lm}^{(3)}$  can be divided into four parts

$$\mathcal{S}_{lm}^{(3)}(\mathbf{x}, \eta) = \mathcal{S}_{lm, \phi\phi\phi}^{(3)}(\mathbf{x}, \eta) + \mathcal{S}_{lm, \phi h_{\phi\phi}}^{(3)}(\mathbf{x}, \eta) + \mathcal{S}_{lm, \phi V_{\phi\phi}}^{(3)}(\mathbf{x}, \eta) + \mathcal{S}_{lm, \phi\psi_{\phi\phi}}^{(3)}(\mathbf{x}, \eta). \quad (2.15)$$

The subscripts in Eq. (2.15) represent the source of SIGWs. For example, the symbol  $\mathcal{S}_{\phi V_{\phi\phi}}^{(3)}$  represents the source term of first order scalar perturbation  $\phi$  and second order scalar induced vector perturbation  $V_{\phi\phi}$ . The explicit expressions of four kinds of source terms in Eq. (2.15) are given by [48]

$$\begin{aligned} \mathcal{S}_{lm, \phi\phi\phi}^{(3)}(\mathbf{x}, \eta) &= 12\phi^{(1)}\partial_l\phi^{(1)}\partial_m\phi^{(1)} - \frac{4}{\mathcal{H}}\phi^{(1)'}\partial_l\phi^{(1)}\partial_m\phi^{(1)} + \frac{2}{3\mathcal{H}^2}\Delta\phi^{(1)}\partial_l\phi^{(1)}\partial_m\phi^{(1)} \\ &+ \frac{2}{3\mathcal{H}^4}\Delta\phi^{(1)}\partial_l\phi^{(1)'}\partial_m\phi^{(1)'} - \frac{3}{\mathcal{H}^2}\phi^{(1)'}\partial_l\phi^{(1)'}\partial_m\phi^{(1)} - \frac{3}{\mathcal{H}^2}\phi^{(1)'}\partial_m\phi^{(1)'}\partial_l\phi^{(1)} \\ &+ \frac{2}{3\mathcal{H}^3}\Delta\phi^{(1)}\partial_l\phi^{(1)'}\partial_m\phi^{(1)} + \frac{2}{3\mathcal{H}^3}\Delta\phi^{(1)}\partial_m\phi^{(1)'}\partial_l\phi^{(1)} \\ &- \frac{2}{\mathcal{H}^3}\phi^{(1)'}\partial_l\phi^{(1)'}\partial_m\phi^{(1)'} - \frac{4}{\mathcal{H}^2}\phi^{(1)}\partial_l\phi^{(1)'}\partial_m\phi^{(1)'}, \end{aligned} \quad (2.16)$$

$$\begin{aligned} \mathcal{S}_{lm, \phi h_{\phi\phi}}^{(3)}(\mathbf{x}, \eta) &= -\frac{1}{2}\phi^{(1)}\left(h_{lm}^{(2)''} + 2\mathcal{H}h_{lm}^{(2)'} - \Delta h_{lm}^{(2)}\right) - \phi^{(1)}\Delta h_{lm}^{(2)} - \phi^{(1)'}\mathcal{H}h_{lm}^{(2)} - \frac{1}{3}\Delta\phi^{(1)}h_{lm}^{(2)} \\ &- \partial^b\phi^{(1)}\partial_b h_{lm}^{(2)}, \end{aligned} \quad (2.17)$$

$$\begin{aligned} \mathcal{S}_{lm, \phi V_{\phi\phi}}^{(3)}(\mathbf{x}, \eta) &= \phi^{(1)}\partial_l\left(V_m^{(2)'} + 2\mathcal{H}V_m^{(2)}\right) + \phi^{(1)}\partial_m\left(V_l^{(2)'} + 2\mathcal{H}V_l^{(2)}\right) + \phi^{(1)'}\left(\partial_l V_m^{(2)} + \partial_m V_l^{(2)}\right) \\ &- \frac{\phi^{(1)}}{8\mathcal{H}}\left(\partial_m\Delta V_l^{(2)} + \partial_l\Delta V_m^{(2)}\right) - \frac{\phi^{(1)'}}{8\mathcal{H}^2}\left(\partial_m\Delta V_l^{(2)} + \partial_l\Delta V_m^{(2)}\right), \end{aligned} \quad (2.18)$$

$$\begin{aligned} \mathcal{S}_{lm, \phi\psi_{\phi\phi}}^{(3)}(\mathbf{x}, \eta) &= \frac{1}{\mathcal{H}}\left(\phi^{(1)}\partial_l\partial_m\psi^{(2)'}\right) + \frac{1}{\mathcal{H}}\left(\phi^{(1)'}\partial_l\partial_m\phi^{(2)}\right) + \frac{1}{\mathcal{H}^2}\left(\phi^{(1)'}\partial_l\partial_m\psi^{(2)'}\right) \\ &+ 3\left(\phi^{(1)}\partial_l\partial_m\phi^{(2)}\right). \end{aligned} \quad (2.19)$$

By solving Eq. (2.14), we obtain the third order SIGWs in momentum space [49]

$$h^{\lambda, (3)}(\mathbf{k}, \eta) = h_{\phi\phi\phi}^{\lambda, (3)}(\mathbf{k}, \eta) + h_{\phi h_{\phi\phi}}^{\lambda, (3)}(\mathbf{k}, \eta) + h_{\phi V_{\phi\phi}}^{\lambda, (3)}(\mathbf{k}, \eta) + h_{\phi\psi_{\phi\phi}}^{\lambda, (3)}(\mathbf{k}, \eta), \quad (2.20)$$

where

$$\begin{aligned} h_{\phi\phi\phi}^{\lambda, (3)}(\mathbf{k}, \eta) &= \int \frac{d^3p}{(2\pi)^{3/2}} \int \frac{d^3q}{(2\pi)^{3/2}} \varepsilon^{\lambda, lm}(\mathbf{k}) q_m (p_l - q_l) \\ &\times I_{\phi\phi\phi}^{(3)}(u, \bar{u}, \bar{v}, x) \zeta_{\mathbf{k}-\mathbf{p}} \zeta_{\mathbf{p}-\mathbf{q}} \zeta_{\mathbf{q}}, \end{aligned} \quad (2.21)$$

$$\begin{aligned} h_{\phi h_{\phi\phi}}^{\lambda, (3)}(\mathbf{k}, \eta) &= \int \frac{d^3p}{(2\pi)^{3/2}} \int \frac{d^3q}{(2\pi)^{3/2}} \varepsilon^{\lambda, lm}(\mathbf{k}) \Lambda_{lm}^{rs}(\mathbf{p}) q_r q_s \\ &\times I_{\phi h_{\phi\phi}}^{(3)}(u, \bar{u}, \bar{v}, x) \zeta_{\mathbf{k}-\mathbf{p}} \zeta_{\mathbf{p}-\mathbf{q}} \zeta_{\mathbf{q}}, \end{aligned} \quad (2.22)$$

$$\begin{aligned} h_{\phi V_{\phi\phi}}^{\lambda, (3)}(\mathbf{k}, \eta) &= \int \frac{d^3p}{(2\pi)^{3/2}} \int \frac{d^3q}{(2\pi)^{3/2}} \varepsilon^{\lambda, lm}(\mathbf{k}) (\mathcal{T}_m^r(\mathbf{p}) p_l + \mathcal{T}_l^r(\mathbf{p}) p_m) \frac{p^s}{p^2} q_r q_s \\ &\times I_{\phi V_{\phi\phi}}^{(3)}(u, \bar{u}, \bar{v}, x) \zeta_{\mathbf{k}-\mathbf{p}} \zeta_{\mathbf{p}-\mathbf{q}} \zeta_{\mathbf{q}}, \end{aligned} \quad (2.23)$$

$$\begin{aligned} h_{\phi\psi_{\phi\phi}}^{\lambda, (3)}(\mathbf{k}, \eta) &= \int \frac{d^3p}{(2\pi)^{3/2}} \int \frac{d^3q}{(2\pi)^{3/2}} \varepsilon^{\lambda, lm}(\mathbf{k}) p_l p_m \\ &\times I_{\phi\psi_{\phi\phi}}^{(3)}(u, \bar{u}, \bar{v}, x) \zeta_{\mathbf{k}-\mathbf{p}} \zeta_{\mathbf{p}-\mathbf{q}} \zeta_{\mathbf{q}}. \end{aligned} \quad (2.24)$$

The explicit expressions of third order kernel functions in Eq. (2.21)–Eq. (2.24) can be found in Refs. [48, 49].

## 2.2 Power spectra of SIGWs

The power spectra of  $n$ -th order gravitational waves (GWs)  $\mathcal{P}_h^{(n)}(\mathbf{k}, \eta)$  are defined as

$$\langle h^{\lambda, (n)}(\mathbf{k}, \eta) h^{\lambda', (n)}(\mathbf{k}', \eta) \rangle = \delta^{\lambda\lambda'} \delta(\mathbf{k} + \mathbf{k}') \frac{2\pi^2}{k^3} \mathcal{P}_h^{(n)}(k, \eta). \quad (2.25)$$

As shown in Eq. (2.25), the power spectrum of GWs can be calculated in terms of the corresponding two-point function. By substituting Eq. (2.13) into Eq. (2.25) and simplifying the momentum integral, we obtain the explicit expression of the power spectra of second order SIGWs

$$\mathcal{P}_h^{(2)}(k, \eta) = 4 \int_0^\infty dv \int_{|1-v|}^{1+v} du \left( \frac{4v^2 - (1 + v^2 - u^2)^2}{4vu} \right)^2 \left( I_h^{(2)}(v, u, x) \right)^2 \mathcal{P}_\zeta(kv) \mathcal{P}_\zeta(ku), \quad (2.26)$$

where we have set  $|\mathbf{k} - \mathbf{p}| = u|\mathbf{k}|$ ,  $|\mathbf{p}| = v|\mathbf{k}|$ , and  $x = |\mathbf{k}|\eta$ .  $\mathcal{P}_\zeta(k)$  is the power spectrum of primordial curvature perturbation which is defined as  $\langle \zeta_{\mathbf{k}} \zeta_{\mathbf{k}'} \rangle = \frac{2\pi^2}{k^3} \delta(\mathbf{k} + \mathbf{k}') \mathcal{P}_\zeta(k)$ . As shown in Fig. 1, the two-point function of second order SIGWs corresponds to two equivalent one-loop diagrams in cosmological perturbation theory.

Similarly, the explicit expression of the power spectra of third order SIGWs can be obtained by using Eq. (2.20) and Eq. (2.25)

$$\mathcal{P}_h^{(3)}(k, \eta) = \sum_{i,j} \mathcal{P}_{ij}^{(3)} \sim \sum_{i,j} \langle h_i^{\lambda, (3)}(\mathbf{k}, \eta) h_j^{\lambda', (3)}(\mathbf{k}', \eta) \rangle, \quad (i, j = \phi\phi\phi, \phi h_{\phi\phi}, \phi V_{\phi\phi}, \phi\psi_{\phi\phi}), \quad (2.27)$$

where the subscripts  $i, j$  in Eq. (2.27) represent the four kinds of source terms of third order SIGWs in Eq. (2.21)–Eq. (2.24). More precisely, we will encounter the following sixteen terms in Eq. (2.27) when calculating the power spectra of third order SIGWs [48]

$$\begin{aligned} \mathcal{P}_{ij}^{(3)} &= \frac{1}{2\pi} \int_0^\infty dv \int_0^\infty d\bar{v} \int_{|1-\bar{v}v|}^{1+\bar{v}v} dw \int_{|1-v|}^{1+v} du \int_{\bar{u}_-}^{\bar{u}_+} d\bar{u} \left\{ \frac{w}{u^2 \bar{u}^2 v \bar{v}^2 \sqrt{Y} (1 - X^2)} \right. \\ &\quad \left. \times I_i^{(3)}(u, v, \bar{u}, \bar{v}, x) \sum_{a=1}^6 \mathbb{P}_{ij}^a(\mathbf{k}, \mathbf{p}, \mathbf{q}) I_{j,a}^{(3)}(u, v, \bar{u}, \bar{v}, w, x) P_\zeta(ku) P_\zeta(k\bar{u}v) P_\zeta(k\bar{v}v) \right\}, \quad (2.28) \\ &\quad (i, j = \phi\phi\phi, \phi h_{\phi\phi}, \phi V_{\phi\phi}, \phi\psi_{\phi\phi}), \end{aligned}$$

where

$$\begin{aligned} \bar{u}_\pm &= \left( 1 + \bar{v}^2 - \frac{(1 + v^2 - u^2)(1 + (\bar{v}v)^2 - w^2)}{2v^2} \right. \\ &\quad \left. \pm 2\bar{v} \sqrt{\left( 1 - \left( \frac{1 + v^2 - u^2}{2v} \right)^2 \right) \left( 1 - \left( \frac{1 + (\bar{v}v)^2 - w^2}{2\bar{v}v} \right)^2 \right)} \right)^{\frac{1}{2}}, \quad (2.29) \end{aligned}$$

$$\begin{aligned} X &= (-1 + u^2 + v^2 - 2\bar{u}^2 v^2 + v^2 \bar{v}^2 + u^2 v^2 \bar{v}^2 - v^4 \bar{v}^2 + w^2 - u^2 w^2 + v^2 w^2) \\ &\quad \times (1 - 2u^2 + u^4 - 2v^2 - 2u^2 v^2 + v^4) (1 - 2v^2 \bar{v}^2 + v^4 \bar{v}^4 - 2w^2 - 2v^2 \bar{v}^2 w^2 + w^4)^{-\frac{1}{2}}, \\ Y &= (1 - 2u^2 + u^4 - 2v^2 - 2u^2 v^2 + v^4) (1 - 2v^2 \bar{v}^2 + v^4 \bar{v}^4 - 2w^2 - 2v^2 \bar{v}^2 w^2 + w^4). \end{aligned}$$

In Eq. (2.28), we have set  $|\mathbf{p} - \mathbf{q}| = \bar{u}|\mathbf{p}|$ ,  $|\mathbf{k} - \mathbf{q}| = w|\mathbf{k}|$ , and  $|\mathbf{q}| = \bar{v}|\mathbf{p}|$ . The corresponding two-loop diagrams in cosmological perturbation theory are given in Appendix C.

The summation of index  $a$  in Eq. (2.28) originates from the Wick's expansions of the six-point function of  $\zeta_{\mathbf{k}}$  in Appendix. B. More precisely, the sum of the six terms ( $a = 1, \dots, 6$ ) in Eq. (2.28) corresponds to the six terms in the Wick's expansions in Eq. (B.1). After integrating the three-dimensional delta functions in the Wick's theorem expansion, we can replace the momenta  $\mathbf{k}'$ ,  $\mathbf{p}'$ , and  $\mathbf{q}'$  with linear combinations of momenta  $\mathbf{k}$ ,  $\mathbf{p}$ , and  $\mathbf{q}$ . In Eq. (2.28), the two multiplied kernel functions can be represented as  $I_i^{(3)}(|\mathbf{k} - \mathbf{p}|, |\mathbf{p} - \mathbf{q}|, |\mathbf{q}|, \eta)$  and  $I_j^{(3)}(|\mathbf{k}' - \mathbf{p}'|, |\mathbf{p}' - \mathbf{q}'|, |\mathbf{q}'|, \eta)$ . It can be observed that since the parameters of the kernel function  $I_i^{(3)}(|\mathbf{k} - \mathbf{p}|, |\mathbf{p} - \mathbf{q}|, |\mathbf{q}|, \eta)$  only contain  $\mathbf{k}$ ,  $\mathbf{p}$ , and  $\mathbf{q}$ , the variable replacement in the Wick expansion will only affect the kernel function  $I_j^{(3)}$ . Therefore, the kernel function  $I_j^{(3)}$  needs to be transformed into  $I_{j,a}^{(3)}$  and summed over the upper index  $a$ , which corresponds to summing over the six terms in Wick's expansion. The detailed discussions can be found in Refs. [48, 52].

The momentum polynomials  $\mathbb{P}_{ij}^a(\mathbf{k}, \mathbf{p}, \mathbf{q})$  in Eq. (2.28) can be calculated in terms of the formal expressions of third order SIGWs in Eq. (2.21)–Eq. (2.24). The explicit expressions of  $\mathbb{P}_{ij}^a(\mathbf{k}, \mathbf{p}, \mathbf{q})$  for  $i, j = \phi\phi\phi, \phi h_{\phi\phi}, \phi V_{\phi\phi}$ , and  $\phi\psi_{\phi\phi}$  are given in Table. 1. Similarly, the superscript  $a = 1, \dots, 6$  in  $\mathbb{P}_{ij}^a$  represents the six terms in Wick's expansion. The momentum polynomials  $\mathbb{P}_{ij}^a$  in Table. 1 can be calculated directly in a given coordinate system using the expression for the polarization tensor in Appendix. A. It should be emphasized that it can also be calculated without selecting a specific coordinate system by using the relationship between the polarization tensor  $\varepsilon^{\lambda,lm}(\mathbf{k})$  and the transverse traceless operator  $\Lambda_{rs}^{lm}(\mathbf{k})$ . Specifically, the polarization tensor satisfies the following expression

$$\delta^{\lambda\bar{\lambda}} \varepsilon^{\bar{\lambda},lm}(\mathbf{k}) \varepsilon^{\bar{\lambda}}_{ij}(\mathbf{k}) = \Lambda_{ij}^{lm}(\mathbf{k}) + A_{ij}^{lm}(\mathbf{k}), \quad (2.30)$$

where  $A_{ij}^{lm}(\mathbf{k})$  is defined as

$$A_{ij}^{lm}(\mathbf{k}) \equiv \frac{1}{\sqrt{2}} (\bar{e}_i(\mathbf{k}) e_j(\mathbf{k}) - e_i(\mathbf{k}) \bar{e}_j(\mathbf{k})) \frac{1}{\sqrt{2}} (\bar{e}_m(\mathbf{k}) e_l(\mathbf{k}) - e_m(\mathbf{k}) \bar{e}_l(\mathbf{k})). \quad (2.31)$$

Since  $A_{ij}^{lm}(\mathbf{k})$  is dependent on the polarization vectors  $\bar{e}_l(\mathbf{k})$  and  $e_l(\mathbf{k})$ , it appears that we still need to select a specific coordinate system when calculating the contraction of the polarization tensor with respect to  $\lambda$  and  $\bar{\lambda}$ . However, as shown in Eq. (2.31),  $A_{ij}^{lm}(\mathbf{k})$  is an antisymmetric tensor, it satisfies  $A_{ij}^{lm} T_{lm} = A_{ij}^{lm} T^{ij} = 0$  for arbitrary symmetric tensor  $T_{ij}$ . Therefore, when  $A_{ij}^{lm}(\mathbf{k})$  acts on a symmetric tensor, we obtain

$$\begin{aligned} \delta^{\lambda\bar{\lambda}} \varepsilon^{\bar{\lambda},lm}(\mathbf{k}) \varepsilon^{\bar{\lambda}}_{ij}(\mathbf{k}) &= \Lambda_{ij}^{lm}(\mathbf{k}) = \mathcal{T}_i^l \mathcal{T}_j^m - \frac{1}{2} \mathcal{T}_{ij} \mathcal{T}^{lm} \\ &= \left( \delta_i^l - \frac{k^l k_i}{|\mathbf{k}|^2} \right) \left( \delta_j^m - \frac{k^m k_j}{|\mathbf{k}|^2} \right) - \frac{1}{2} \left( \delta_{ij} - \frac{k_i k_j}{|\mathbf{k}|^2} \right) \left( \delta^{lm} - \frac{k^l k^m}{|\mathbf{k}|^2} \right). \end{aligned} \quad (2.32)$$

As shown in Eq. (2.32), we can calculate the contraction of the polarization tensor with respect to  $\lambda$  and  $\bar{\lambda}$  without specifying a particular coordinate system. This allows us to simplify the momentum polynomials  $\mathbb{P}_{ij}^a(\mathbf{k}, \mathbf{p}, \mathbf{q})$  without selecting a coordinate system. However, it is important to note that this method is only applicable when  $A_{ij}^{lm}(\mathbf{k})$  acts on a symmetric tensor.

### 3 Energy density spectrum with lognormal primordial power spectrum

The energy density spectrum of SIGWs is defined as

$$\bar{\Omega}_{\text{GW}}(\eta, k) = \frac{\overline{\rho_{\text{GW}}(\eta, k)}}{\rho_{\text{tot}}(\eta)} = \frac{x^2}{6} \overline{\mathcal{P}_h(\eta, k)}, \quad (3.1)$$

where

$$\mathcal{P}_h(\eta, k) = \frac{1}{4} \mathcal{P}_h^{(2)}(\eta, k) + \frac{1}{36} \mathcal{P}_h^{(3)}(\eta, k) + O(\mathcal{P}_h^{(4)}), \quad (3.2)$$

$\mathbb{P}_{ij}^a$	$i = \phi\phi\phi$
$j = \phi\phi\phi$	$\delta^{\lambda\lambda'} (\varepsilon^{\lambda,lm}(\mathbf{k})q_m (p_l - q_l)) \left( \varepsilon^{\lambda',rs}(\mathbf{k}')q'_s (p'_r - q'_r) \right)$
$j = \phi h_{\phi\phi}$	$\delta^{\lambda\lambda'} (\varepsilon^{\lambda,lm}(\mathbf{k})q_m (p_l - q_l)) \left( \varepsilon^{\lambda',bc}(\mathbf{k}')\Lambda_{bc}^{rs}(\mathbf{p}')q'_r q'_s \right)$
$j = \phi V_{\phi\phi}$	$\delta^{\lambda\lambda'} (\varepsilon^{\lambda,lm}(\mathbf{k})q_m (p_l - q_l)) \left( \varepsilon^{\lambda',bc}(\mathbf{k}') (\mathcal{T}_c^r(\mathbf{p}')p'_b + \mathcal{T}_b^r(\mathbf{p}')p'_c) \frac{p'^s}{p'^2} q'_r q'_s \right)$
$j = \phi\psi_{\phi\phi}$	$\delta^{\lambda\lambda'} (\varepsilon^{\lambda,lm}(\mathbf{k})q_m (p_l - q_l)) \left( \varepsilon^{\lambda',rs}(\mathbf{k}')p'_r p'_s \right)$
$\mathbb{P}_{ij}^a$	$i = \phi h_{\phi\phi}$
$j = \phi\phi\phi$	$\delta^{\lambda\lambda'} \left( \varepsilon^{\lambda,lm}(\mathbf{k})\Lambda_{lm}^{ef}(\mathbf{p})q_e q_f \right) \left( \varepsilon^{\lambda',rs}(\mathbf{k}')q'_s (p'_r - q'_r) \right)$
$j = \phi h_{\phi\phi}$	$\delta^{\lambda\lambda'} \left( \varepsilon^{\lambda,lm}(\mathbf{k})\Lambda_{lm}^{ef}(\mathbf{p})q_e q_f \right) \left( \varepsilon^{\lambda',bc}(\mathbf{k}')\Lambda_{bc}^{rs}(\mathbf{p}')q'_r q'_s \right)$
$j = \phi V_{\phi\phi}$	$\delta^{\lambda\lambda'} \left( \varepsilon^{\lambda,lm}(\mathbf{k})\Lambda_{lm}^{ef}(\mathbf{p})q_e q_f \right) \left( \varepsilon^{\lambda',bc}(\mathbf{k}') (\mathcal{T}_c^r(\mathbf{p}')p'_b + \mathcal{T}_b^r(\mathbf{p}')p'_c) \frac{p'^s}{p'^2} q'_r q'_s \right)$
$j = \phi\psi_{\phi\phi}$	$\delta^{\lambda\lambda'} \left( \varepsilon^{\lambda,lm}(\mathbf{k})\Lambda_{lm}^{ef}(\mathbf{p})q_e q_f \right) \left( \varepsilon^{\lambda',rs}(\mathbf{k}')p'_r p'_s \right)$
$\mathbb{P}_{ij}^a$	$i = \phi V_{\phi\phi}$
$j = \phi\phi\phi$	$\delta^{\lambda\lambda'} \left( \varepsilon^{\lambda,lm}(\mathbf{k}) (\mathcal{T}_m^e(\mathbf{p})p_l + \mathcal{T}_l^e(\mathbf{p})p_m) \frac{p^f}{p^2} q_e q_f \right) \left( \varepsilon^{\lambda',rs}(\mathbf{k}')q'_s (p'_r - q'_r) \right)$
$j = \phi h_{\phi\phi}$	$\delta^{\lambda\lambda'} \left( \varepsilon^{\lambda,lm}(\mathbf{k}) (\mathcal{T}_m^e(\mathbf{p})p_l + \mathcal{T}_l^e(\mathbf{p})p_m) \frac{p^f}{p^2} q_e q_f \right) \left( \varepsilon^{\lambda',bc}(\mathbf{k}')\Lambda_{bc}^{rs}(\mathbf{p}')q'_r q'_s \right)$
$j = \phi V_{\phi\phi}$	$\delta^{\lambda\lambda'} \left( \varepsilon^{\lambda,lm}(\mathbf{k}) (\mathcal{T}_m^e(\mathbf{p})p_l + \mathcal{T}_l^e(\mathbf{p})p_m) \frac{p^f}{p^2} q_e q_f \right) \left( \varepsilon^{\lambda',bc}(\mathbf{k}') (\mathcal{T}_c^r(\mathbf{p}')p'_b + \mathcal{T}_b^r(\mathbf{p}')p'_c) \frac{p'^s}{p'^2} q'_r q'_s \right)$
$j = \phi\psi_{\phi\phi}$	$\delta^{\lambda\lambda'} \left( \varepsilon^{\lambda,lm}(\mathbf{k}) (\mathcal{T}_m^e(\mathbf{p})p_l + \mathcal{T}_l^e(\mathbf{p})p_m) \frac{p^f}{p^2} q_e q_f \right) \left( \varepsilon^{\lambda',rs}(\mathbf{k}')p'_r p'_s \right)$
$\mathbb{P}_{ij}^a$	$i = \phi\psi_{\phi\phi}$
$j = \phi\phi\phi$	$\delta^{\lambda\lambda'} (\varepsilon^{\lambda,lm}(\mathbf{k})p_l p_m) \left( \varepsilon^{\lambda',rs}(\mathbf{k}')q'_s (p'_r - q'_r) \right)$
$j = \phi h_{\phi\phi}$	$\delta^{\lambda\lambda'} (\varepsilon^{\lambda,lm}(\mathbf{k})p_l p_m) \left( \varepsilon^{\lambda',bc}(\mathbf{k}')\Lambda_{bc}^{rs}(\mathbf{p}')q'_r q'_s \right)$
$j = \phi V_{\phi\phi}$	$\delta^{\lambda\lambda'} (\varepsilon^{\lambda,lm}(\mathbf{k})p_l p_m) \left( \varepsilon^{\lambda',bc}(\mathbf{k}') (\mathcal{T}_c^r(\mathbf{p}')p'_b + \mathcal{T}_b^r(\mathbf{p}')p'_c) \frac{p'^s}{p'^2} q'_r q'_s \right)$
$j = \phi\psi_{\phi\phi}$	$\delta^{\lambda\lambda'} (\varepsilon^{\lambda,lm}(\mathbf{k})p_l p_m) \left( \varepsilon^{\lambda',rs}(\mathbf{k}')p'_r p'_s \right)$

**Table 1:** The explicit expressions of momentum polynomials  $\mathbb{P}_{ij}^a(\mathbf{k}, \mathbf{p}, \mathbf{q})$ .

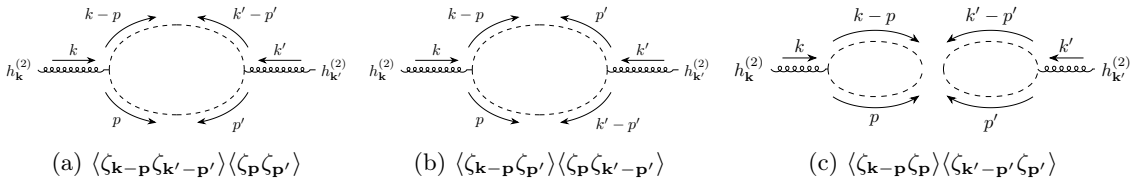


**Figure 1:** The diagrams correspond to the Wick's expansions of four-point correlation function. The dashed and spring-like lines in the figure represent scalar and tensor perturbations, respectively. Diagram (a) and diagram (b) correspond to the nontrivial contributions of the power spectrum of second order SIGWs in Eq. (2.26).

is the total power spectrum of SIGWs. The overline represents the oscillation average. The total energy density spectrum of SIGWs up to third order can be represented as

$$\begin{aligned}
\bar{\Omega}_{\text{GW}}^{\text{tot}}(\eta, k) &= \bar{\Omega}_{\text{GW}}^{(2)}(\eta, k) + \bar{\Omega}_{\text{GW}}^{(3)}(\eta, k) \\
&= \bar{\Omega}_{\text{GW}}^{(2)}(\eta, k) + \sum_{i,j} \bar{\Omega}_{ij}^{(3)}(\eta, k), \quad (i, j = \phi\phi\phi, \phi h_{\phi\phi}, \phi V_{\phi\phi}, \phi\psi_{\phi\phi}), \quad (3.3)
\end{aligned}$$



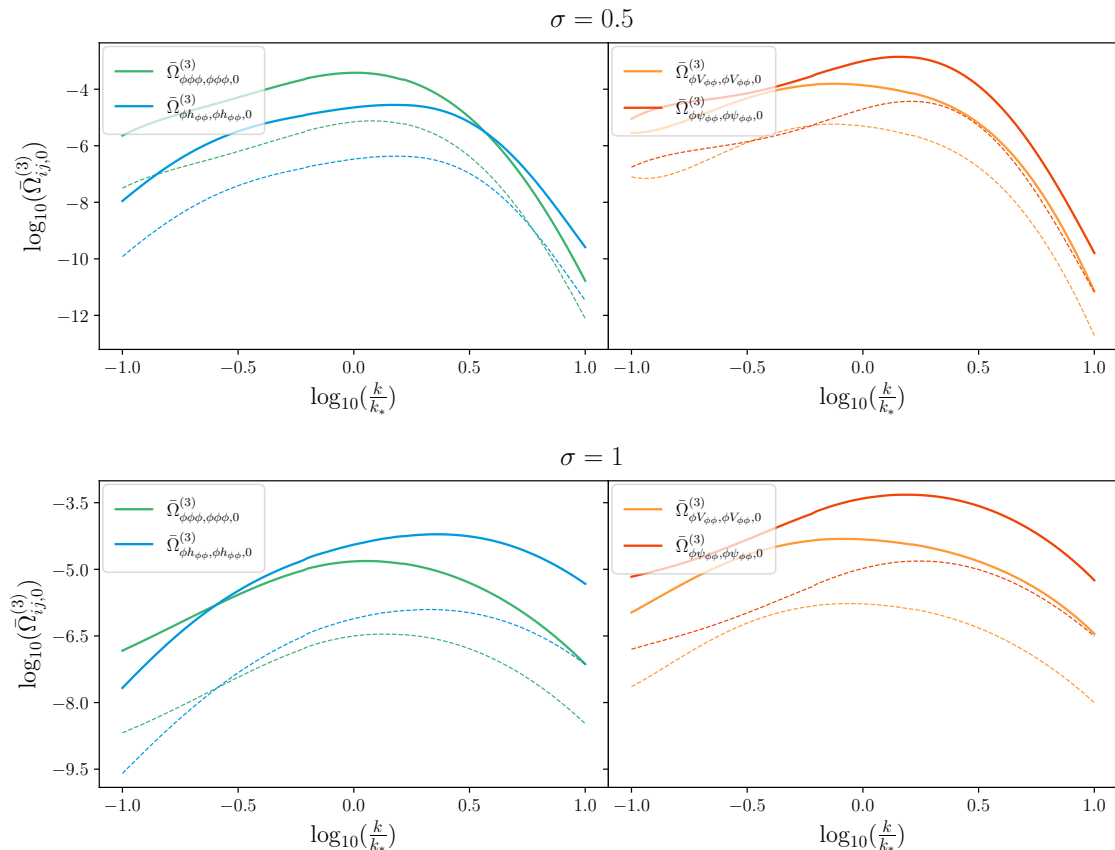


**Figure 2:** The energy density spectra of third order SIGWs for different kinds of source terms:  $\bar{\Omega}_{ij,0}^{(3)}(k)$  with  $i = j$ . We set  $A_\zeta = 1$  and  $\sigma = 0.5, 1$ . The solid lines represent the result of the power spectrum and the corresponding dashed lines represent the error in the calculation of the corresponding power spectrum.

where  $\bar{\Omega}_{\text{GW}}^{(2)}(\eta, k)$  and  $\bar{\Omega}_{\text{GW}}^{(3)}(\eta, k)$  represent the energy density spectra of second and third order SIGWs, respectively. Taking into account the thermal history of the universe, we obtain the current total energy density spectrum [54]

$$\bar{\Omega}_{\text{GW},0}^{\text{tot}}(k) = \Omega_{\text{rad},0} \left( \frac{g_{*,\rho,e}}{g_{*,\rho,0}} \right) \left( \frac{g_{*,s,0}}{g_{*,s,e}} \right)^{4/3} \bar{\Omega}_{\text{GW}}^{\text{tot}}(\eta, k), \quad (3.4)$$

where  $\Omega_{\text{rad},0} (= 4.2 \times 10^{-5} h^{-2})$  is the energy density fraction of radiations today, and the dimensionless Hubble constant is  $h = 0.6736$  [55]. The effect numbers of relativistic species  $g_{*,\rho}$  and  $g_{*,s}$  can be found in Ref. [56]. In this paper, we extend the results of Refs. [48] to the log-normal primordial power spectrum

$$\mathcal{P}_\zeta(k) = \frac{A_\zeta}{\sqrt{2\pi\sigma^2}} \exp\left(-\frac{\ln^2(k/k_*)}{2\sigma^2}\right), \quad (3.5)$$

where  $A_\zeta$  is the amplitude of primordial power spectrum and  $k_* = 2\pi f_*$  is the wavenumber at which the primordial power spectrum has a log-normal peak. Following Eq. (2.28), we numerically calculate the energy density spectra of third order SIGWs using `vegas` package [57–59]. The numerical results of third order energy density spectra  $\bar{\Omega}_{ij,0}^{(3)}(k)$  with  $i = j$  are shown in Fig. 2. Since `vegas` uses a Monte Carlo integration strategy, it is necessary to analyze the errors in our calculations. As depicted in Fig. 2, we present the computed results for the third order energy density spectrum using solid lines, while the corresponding numerical calculation errors

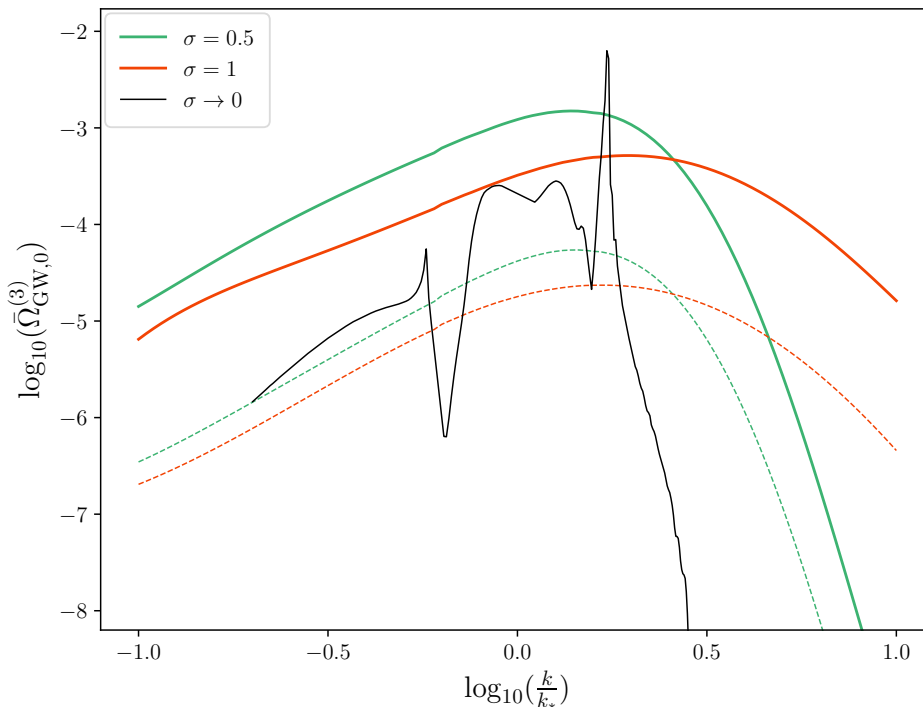


**Figure 3:** The energy density spectra of third order SIGWs  $\bar{\Omega}_{\text{GW},0}^{(3)}(k)$ . The black line represents the result of monochromatic primordial power spectrum in Ref. [48]. The green and red lines represent the cases of log-normal primordial power spectra with  $\sigma = 0.5$  and  $\sigma = 1$ , respectively. The solid line is the result of the power spectrum and the dashed line of the same color indicates the error in the calculation of the corresponding power spectrum.

are represented by dashed lines of the same color. Notably, the numerical integration error is negligible compared to the computed values. Moreover, in the case of a monochromatic primordial power spectrum, the second order vector perturbation induced by the first order scalar perturbation is zero [52]. This implies that source term  $\phi V_{\phi\phi}$  does not contribute to the third order SIGWs [48]. However, as shown by the orange solid line in Fig. 2, considering a log-normal primordial power spectrum, we find that non-zero second order vector perturbations can impact the third order SIGWs.

The energy density spectra of third order SIGWs  $\bar{\Omega}_{\text{GW},0}^{(3)}(k)$  for different  $\sigma$  are shown in Fig. 3. As  $\sigma$  gradually increases, the energy density spectrum of third-order gravitational waves widens progressively. In addition, the total power spectrum of the second order and third order SIGWs  $\bar{\Omega}_{\text{GW},0}^{\text{tot}}(k)$  ( $= \bar{\Omega}_{\text{GW},0}^{(2)}(k) + \bar{\Omega}_{\text{GW},0}^{(3)}(k)$ ) is plotted in Fig. 4. As depicted, even for  $A_\zeta = 10^{-2}$ , the third order SIGWs still impact a noticeable correction to the total power spectrum. When  $A_\zeta = 10^{-3}$ , the impact of third order SIGWs diminishes. Furthermore, the results presented in Fig. 4 indicate that the substantial contribution of third order SIGWs to the total energy density spectrum in the high-frequency region ( $\tilde{k} = k/k_* > 0.1$ ) is not solely due to the peculiar nature of the monochromatic primordial power spectrum. Even when considering a more realistic broadened primordial power spectrum, third order SIGWs continue to exert a significant impact on the total energy density spectrum.

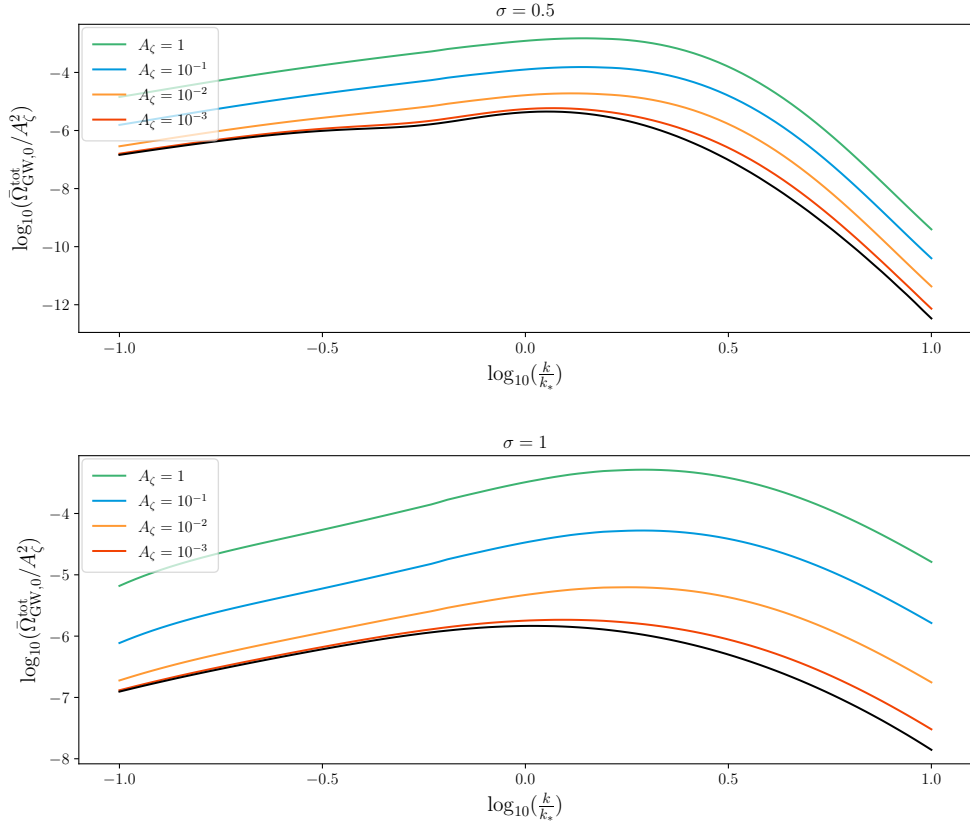


**Figure 4:** The total energy density spectra of SIGWs  $\bar{\Omega}_{\text{GW},0}^{\text{tot}}(k)/A_\zeta^2$  for different values of  $A_\zeta$ . The black line represents the energy density of second order SIGWs  $\bar{\Omega}_{\text{GW},0}^{(2)}(k)/A_\zeta^2$ .

## 4 Detection of SIGWs

In this section, we analyze the SNR of LISA and also apply our results to a Bayesian analysis of the PTA data in the case where SIGWs dominates SGWBs in the LISA and PTA bands respectively.

### 4.1 Signal-to-noise ratio of LISA

In order to explore the effect of third order SIGWs on high-frequency region ( $\tilde{k} = k/k_* > 0.1$ ), we calculate the SNR  $\rho$  for LISA [60–62]

$$\rho = \sqrt{T} \left[ \int df \left( \frac{\bar{\Omega}_{\text{GW},0}(f)}{\Omega_n(f)} \right)^2 \right]^{1/2}, \quad (4.1)$$

where  $T$  is the observation time and we set  $T = 4$  years here.  $\Omega_n(f) = 2\pi^2 f^3 S_n / 3H_0^2$ , where  $H_0$  is the Hubble constant,  $S_n$  is the strain noise power spectral density [61]. In Fig. 5, we plot the SNR curves for LISA experiments.  $\rho^{(2)}$  and  $\rho^{\text{tot}} = \rho^{(2)} + \rho^{(3)}$  represent the SNR for the second order contribution and total contribution, respectively. It shows that the third order SIGWs have a large impact in high-frequency region ( $\tilde{k} > 0.1$ ) and can produce a 70% SNR boost when  $A_\zeta = 0.02$ . Fig. 6 shows the variation of the SNR with  $A_\zeta$  for a fixed  $f_*$ . If we tolerate a value of  $A_\zeta$  as high as  $A_\zeta \sim 0.1$ , then the SNR can even be improved by 400% at  $f_* = 1.3 \times 10^{-3}$  Hz.

Therefore, the substantial contribution of third order SIGWs in high-frequency region ( $\tilde{k} > 0.1$ ) is not solely a consequence of the special nature of monochromatic primordial power spectrum. Their impact remains significant even when considering realistic power spectra.

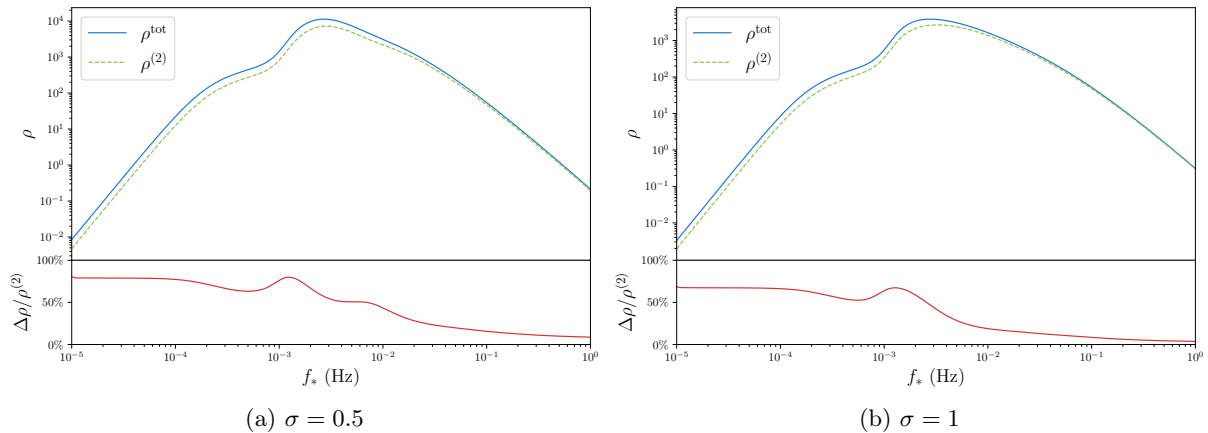


**Figure 5:** The SNR as a function of frequency for LISA experiment for both the second order SIGWs  $\rho^{(2)}$  and the total SIGWs  $\rho^{\text{tot}} = \rho^{(2)} + \rho^{(3)}$  with a fixed value of  $A_\zeta = 0.02$ . The curves below show the improvement of SNR after considering the third order SIGWs.

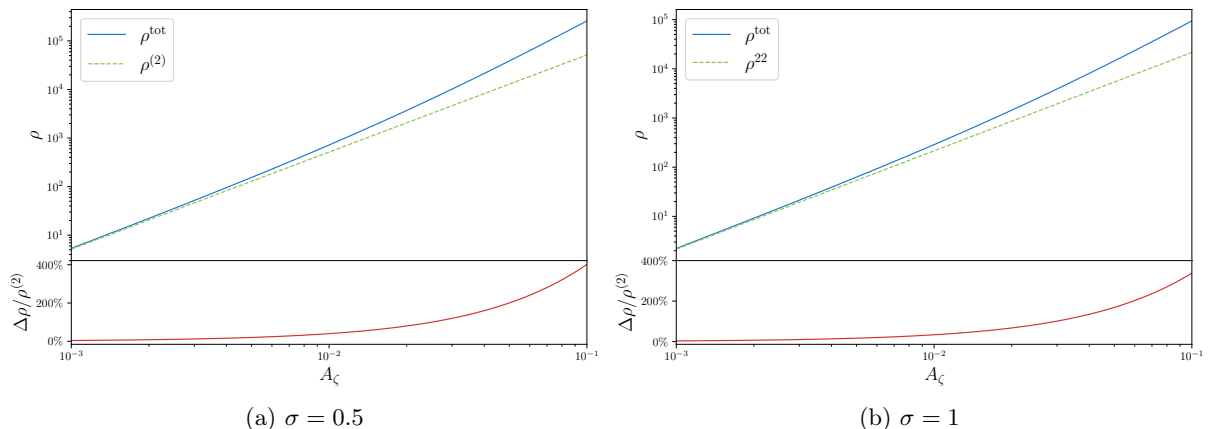


**Figure 6:** The SNR as a function of frequency for LISA experiment for both the second order SIGWs  $\rho^{(2)}$  and the total SIGWs  $\rho^{\text{tot}} = \rho^{(2)} + \rho^{(3)}$  with a fixed value of  $f_* = 1.3 \times 10^{-3}$  Hz. The curves below show the improvement of SNR after considering the third order SIGWs.

## 4.2 PTA observations

In order to constrain the parameter space of primordial power spectrum in terms of PTA observations, we use Ceffyl [63] package embedded in PTArade [64] to analyze the data from the first 14 frequency bins of NANOGrav 15-year and the first 9 frequency bins in EPTA DR2 new. We show the posteriors distributions in Fig. 7, where the priors distributions of  $\log(f_*/\text{Hz})$  and  $\log(A_\zeta)$  are set as uniform distributions over the intervals  $[-9, -6]$  and  $[-3, 1]$ , respectively. Analyzing the posterior distributions of second order SIGWs energy density spectrum  $\bar{\Omega}_{\text{GW},0}^{(2)}(k)$  as well as the total energy density spectrum  $\bar{\Omega}_{\text{GW},0}^{\text{tot}}(k) \left( = \bar{\Omega}_{\text{GW},0}^{(2)}(k) + \bar{\Omega}_{\text{GW},0}^{(3)}(k) \right)$ , we find that, in low-frequency regime ( $\tilde{k} < 0.1$ ), the effect of the third order SIGWs is smaller than in high-frequency region. The median values of  $\log(A_\zeta)$  and  $\log(f_*/\text{Hz})$  become smaller when considering the effects of third order SIGWs. More precisely,

1. For  $\sigma = 0.5$ , in the case of NANOGrav 15-year data only, the median value of  $\log(A_\zeta)$  goes from  $-0.9$  to  $-1.3$  and the median value of  $\log(f_*/\text{Hz})$  goes from  $-7.2$  to  $-7.5$ . In the case of joint data from NANOGrav 15-year and EPTA DR2 new, the median value of  $\log(A_\zeta)$  goes from  $-0.7$  to  $-1.1$  and the median value of  $\log(f_*/\text{Hz})$  goes from  $-7.0$  to  $-7.3$ .
2. For  $\sigma = 1$ , in the case of NANOGrav 15-year data only, the median value of  $\log(A_\zeta)$  goes from  $-0.7$  to  $-1.0$  and the median value of  $\log(f_*/\text{Hz})$  goes from  $-7.0$  to  $-7.2$ . In the case of joint data from NANOGrav 15-year and EPTA DR2 new, the median value of  $\log(A_\zeta)$  goes from  $-0.4$  to  $-0.8$  and the median value of  $\log(f_*/\text{Hz})$  goes from  $-6.8$  to  $-7.0$ .

In Fig. 8, we plot the total energy density spectra  $\bar{\Omega}_{\text{GW},0}^{\text{tot}}(k)$  and compare the results with the case of second order SIGWs.

## 5 Conclusion and discussion

In this paper, we systematically investigated the third order SIGWs with log-normal primordial power spectra. Our results reveal that the third order SIGWs have a significant impact on the total energy density spectrum of GWs. More precisely, their contribution is most pronounced in the high-frequency region of the energy density spectrum. As depicted in Fig.4, the presence of third order SIGWs alters the shape of the energy density spectrum at high frequencies. Quantifying their influence, we computed the SNR for the LISA frequency band. Remarkably, when the amplitude of the primordial power spectrum  $A_\zeta = 0.02$ , third order SIGWs enhance the SNR of LISA by approximately 70%. However, in the low-frequency regime of the total gravitational wave energy density spectrum, their contribution is relatively small, as shown in Fig. 7. Combining this with observational data from PTA, we find that third order SIGWs also impact the amplitude  $A_\zeta$  and peak position  $f_*$  of the log-normal primordial power spectrum. In summary, we conclude that the substantial contribution of third order SIGWs is not solely a consequence of the special nature of monochromatic primordial power spectrum. Their impact remains significant even when considering realistic primordial power spectra.

The energy density spectrum of third order SIGWs can be obtained by calculating the two-point correlation function of third order SIGWs. As shown in Appendix. C, the two-point correlation function of third order SIGWs corresponds to the two-loop diagrams proportional to  $A_\zeta^3$  in cosmological perturbation theory. It is important to note that the two-point correlation function of fourth order SIGWs and second order SIGWs  $\langle h_{\mathbf{k}}^{\lambda,(4)} h_{\mathbf{k}'}^{\lambda',(2)} \rangle$  can still provide a two-loop contribution proportional to  $A_\zeta^3$ . Since the contribution of the two-point correlation function  $\langle h_{\mathbf{k}}^{\lambda,(4)} h_{\mathbf{k}'}^{\lambda',(2)} \rangle$  is also proportional to  $A_\zeta^3$ , it may also have a significant contribution to the total energy density spectrum of GWs. However, due to the complexity of the calculation of fourth order SIGWs, the calculations of the two-loop contributions of SIGWs waves have not yet been completed.

We can observe from the above discussion that the third order SIGWs have a significant impact on the total energy density spectrum of SIGWs. As  $A_\zeta$  increases, the contribution of third order SIGWs can even surpass that of second order ones. This makes it necessary to consider the convergence of the perturbative expansion in the calculation of SIGWs. The total energy density spectrum of SIGWs can be expressed in the following form

$$\begin{aligned}
\Omega_{\text{GW}}(k) = & A_\zeta^2 \left( \Omega_{\text{GW}}^{(2,2)}(k) \right) \Big|_{A_\zeta=1} + A_\zeta^3 \left( \sum_{m=0}^1 \Omega_{\text{GW}}^{(3+m,3-m)}(k) \right) \Big|_{A_\zeta=1} \\
& + A_\zeta^4 \left( \sum_{m=0}^2 \Omega_{\text{GW}}^{(4+m,4-m)}(k) \right) \Big|_{A_\zeta=1} + \dots,
\end{aligned} \tag{5.1}$$

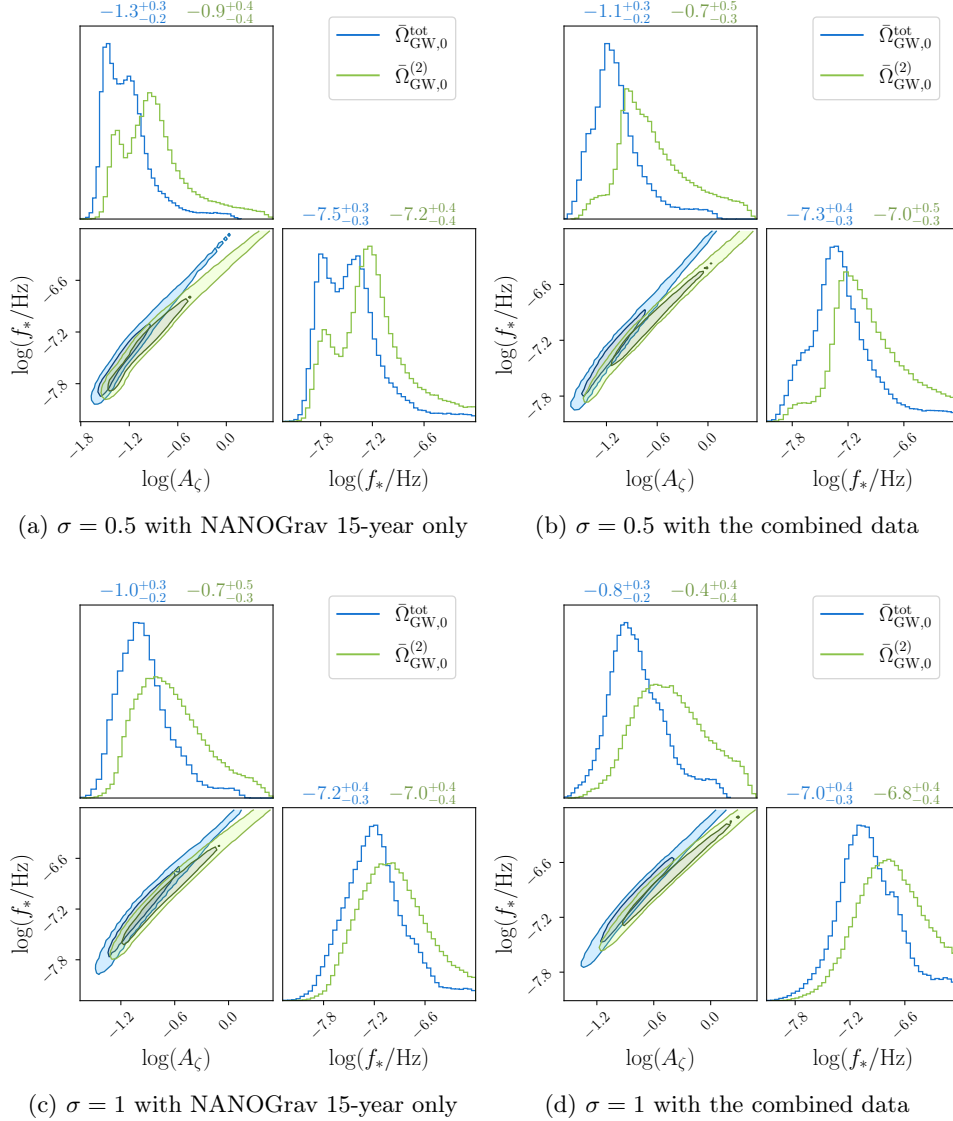


**Figure 7:** The posteriors and  $1\text{-}\sigma$  ranges of two independent parameters  $\log(f_*/\text{Hz})$  and  $\log(A_\zeta)$ . The blue one corresponds to the result of  $\bar{\Omega}_{\text{GW},0}^{\text{tot}}(k)$  ( $= \bar{\Omega}_{\text{GW},0}^{(2)}(k) + \bar{\Omega}_{\text{GW},0}^{(3)}(k)$ ) and the green one corresponds to the result of  $\bar{\Omega}_{\text{GW},0}^{(2)}(k)$  only. The term ‘combined data’ refers to the aggregate dataset encompassing both NANOGrav 15-year and EPTA DR2 new. The numbers above the figures correspond to the median values and  $1\text{-}\sigma$  ranges of the parameters.

where,  $\left(\Omega_{\text{GW}}^{(n,m)}(k)\right)\Big|_{A_\zeta=1}$  denotes the energy density spectrum corresponds to the two-point correlation function  $\langle h_{\mathbf{k}}^{\lambda,(n)} h_{\mathbf{k}'}^{\lambda',(m)} \rangle$  when the amplitude of the primordial power spectrum  $A_\zeta = 1$ . We have denoted  $\Omega_{\text{GW}}^{(n,n)}(k)$  as  $\Omega_{\text{GW}}^{(n)}(k)$  in previous sections. Similar to second and third order SIGWs, the energy density spectrum  $\Omega_{\text{GW}}^{(n,m)}(k)$  can be approximated as

$$\Omega_{\text{GW}}^{(n,m)}(k) \sim \int d^3 p_{n-1} \cdots \int d^3 p_1 \mathbb{P}^{ij} I^{(n)} I^{(m)} \times \mathcal{P}_\zeta(|\mathbf{k} - \mathbf{p}_1|) \cdots \mathcal{P}_\zeta(|\mathbf{p}_{n-2} - \mathbf{p}_{n-1}|) \mathcal{P}_\zeta(|\mathbf{p}_{n-1}|), \quad (5.2)$$

where,  $I^{(n)}$  represents the kernel function of  $n$ -th order SIGWs,  $\mathbb{P}^{ij}$  denotes the momentum polynomial, and  $\mathcal{P}_\zeta(k)$  stands for the primordial power spectrum. Since the observational data

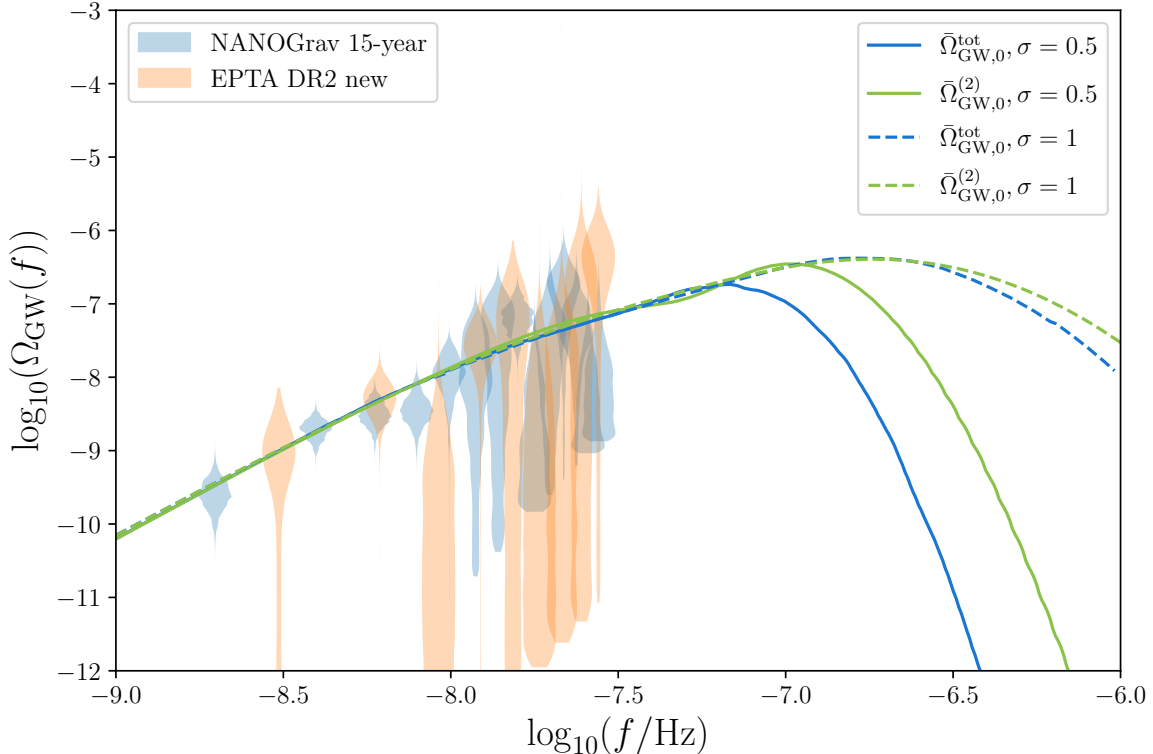


**Figure 8:** The energy density spectra with  $\sigma = 1, 0.5$ . The blue curves correspond to the total density spectra  $\bar{\Omega}_{\text{GW},0}^{\text{tot}}(k) \left( = \bar{\Omega}_{\text{GW},0}^{(2)}(k) + \bar{\Omega}_{\text{GW},0}^{(3)}(k) \right)$  and the green curves correspond to the density spectra of  $\bar{\Omega}_{\text{GW},0}^{(2)}(k)$  only. We select the parameters from subfigures (b) and (d) of Fig. 7. The energy density spectra derived from the free spectrum of NANOGrav 15-year data set and EPTA DR2 new are also shown here.

of PTA suggests that  $A_\zeta$  has a relatively large value, in this case, third order SIGWs will have a more significant contribution compared to second order ones. This motivates us to consider the following three questions:

1. Whether the two-point correlation function  $\langle h_{\mathbf{k}}^{\lambda,(4)} h_{\mathbf{k}'}^{\lambda',(2)} \rangle \sim A_\zeta^{(3)}$  and higher order SIGWs would generate contributions larger than the second and third order SIGWs?
2. How the two-point correlation function  $\langle h_{\mathbf{k}}^{\lambda,(4)} h_{\mathbf{k}'}^{\lambda',(2)} \rangle \sim A_\zeta^{(3)}$  and higher order SIGWs affect the SNR of LISA and the posteriors distributions of  $\log(f_*/\text{Hz})$  and  $\log(A_\zeta)$  in PTA observation?
3. Under what conditions does the perturbative expansion of the SIGWs in Eq. (5.1) converge?

However, without explicit calculations of the energy density spectra of higher order SIGWs, it is difficult to provide precise answers to the above three questions. Detailed calculation of high order SIGWs and convergence of the expansion in Eq. (5.1) requires further research in future work.

In the studies of SIGWs, the GWs are induced by large primordial curvature perturbations on small scales. For primordial tensor perturbations, there are not many observational constraints on small scales either. We can also consider models of large primordial tensor perturbations on small scales [65]. In this case, the primordial curvature perturbation and the primordial tensor perturbation together induce high order GWs. Refs. [66, 67] studied the one-loop contribution of induced GWs in this case. The corresponding two-loop calculation and its constraints on specific inflationary models might be studied in future work.

## Acknowledgments

We thank Dr. Xukun Zhang for useful discussions. This work has been funded by the National Nature Science Foundation of China under grant No. 12075249, 11690022, and 12275276, and the Key Research Program of the Chinese Academy of Sciences under Grant No. XDPB15.

## A Polarization tensors

The polarization tensors for momentum  $\mathbf{k}$  are defined as

$$\varepsilon_{ij}^{\times}(\mathbf{k}) = \frac{1}{\sqrt{2}} (e_i(\mathbf{k}) \bar{e}_j(\mathbf{k}) + \bar{e}_i(\mathbf{k}) e_j(\mathbf{k})) , \quad (\text{A.1})$$

$$\varepsilon_{ij}^{+}(\mathbf{k}) = \frac{1}{\sqrt{2}} (e_i(\mathbf{k}) e_j(\mathbf{k}) - \bar{e}_i(\mathbf{k}) \bar{e}_j(\mathbf{k})) , \quad (\text{A.2})$$

where  $e_i(\mathbf{k})$  and  $\bar{e}_i(\mathbf{k})$  are transverse polarization vectors in three dimensional momentum space. For a given coordinate system, the polarization vectors can be written as

$$\mathbf{k} = (0, 0, k) , \quad e_i(\mathbf{k}) = (1, 0, 0) , \quad \bar{e}_i(\mathbf{k}) = (0, 1, 0) . \quad (\text{A.3})$$

In this coordinate system, the explicit expressions of polarization tensors  $\varepsilon_{ij}^{\lambda}(\mathbf{k})$  ( $\lambda = +, \times$ ) can be obtained in terms of Eq. (A.1). We define  $|\mathbf{k} - \mathbf{p}| = u|\mathbf{k}|$  and  $|\mathbf{p}| = v|\mathbf{k}|$ . Then, the polarization tensors for  $\mathbf{k} - \mathbf{p}$  and  $\mathbf{p}$  are given by

$$\varepsilon_{ij}^{\times}(\mathbf{k} - \mathbf{p}) = \frac{1}{\sqrt{2}} (e_i(\mathbf{k} - \mathbf{p}) \bar{e}_j(\mathbf{k} - \mathbf{p}) + \bar{e}_i(\mathbf{k} - \mathbf{p}) e_j(\mathbf{k} - \mathbf{p})) , \quad (\text{A.4})$$

$$\varepsilon_{ij}^{+}(\mathbf{k} - \mathbf{p}) = \frac{1}{\sqrt{2}} (e_i(\mathbf{k} - \mathbf{p}) e_j(\mathbf{k} - \mathbf{p}) - \bar{e}_i(\mathbf{k} - \mathbf{p}) \bar{e}_j(\mathbf{k} - \mathbf{p})) , \quad (\text{A.5})$$

$$\varepsilon_{ij}^{\times}(\mathbf{p}) = \frac{1}{\sqrt{2}} (e_i(\mathbf{p}) \bar{e}_j(\mathbf{p}) + \bar{e}_i(\mathbf{p}) e_j(\mathbf{p})) , \quad (\text{A.6})$$

$$\varepsilon_{ij}^{+}(\mathbf{p}) = \frac{1}{\sqrt{2}} (e_i(\mathbf{p}) e_j(\mathbf{p}) - \bar{e}_i(\mathbf{p}) \bar{e}_j(\mathbf{p})) , \quad (\text{A.7})$$

where

$$\mathbf{k} - \mathbf{p} = k \left( -\sqrt{v^2 - \frac{1}{4}(-u^2 + v^2 + 1)^2}, 0, \frac{1}{2}(u^2 - v^2 + 1) \right) , \quad (\text{A.8})$$

$$e_i(\mathbf{k} - \mathbf{p}) = \left( \frac{u^2 - v^2 + 1}{2u}, 0, \frac{\sqrt{-u^4 + 2u^2v^2 + 2u^2 - v^4 + 2v^2 - 1}}{2u} \right) , \quad (\text{A.9})$$

$$\bar{e}_i(\mathbf{k} - \mathbf{p}) = (0, 1, 0) , \quad (\text{A.10})$$

$$\mathbf{p} = k \left( \sqrt{v^2 - \frac{1}{4}(-u^2 + v^2 + 1)^2}, 0, \frac{1}{2}(-u^2 + v^2 + 1) \right) , \quad (\text{A.11})$$

$$e_i(\mathbf{p}) = \left( -\frac{-u^2 + v^2 + 1}{2v}, 0, \frac{\sqrt{-u^4 + 2u^2(v^2 + 1) - (v^2 - 1)^2}}{2v} \right) , \quad (\text{A.12})$$

$$\bar{e}_i(\mathbf{p}) = (0, 1, 0) . \quad (\text{A.13})$$



## B Six-point function

The non-trivial terms in Wick's expansions of six-point correlation function are

$$\begin{aligned}
& \langle \zeta_{\mathbf{k}-\mathbf{p}} \zeta_{\mathbf{p}-\mathbf{q}} \zeta_{\mathbf{q}} \zeta_{\mathbf{k}'-\mathbf{p}'} \zeta_{\mathbf{p}'-\mathbf{q}'} \zeta_{\mathbf{q}'} \rangle \\
&= \langle \zeta_{\mathbf{k}-\mathbf{p}} \zeta_{\mathbf{k}'-\mathbf{p}'} \rangle \langle \zeta_{\mathbf{p}-\mathbf{q}} \zeta_{\mathbf{p}'-\mathbf{q}'} \rangle \langle \zeta_{\mathbf{q}} \zeta_{\mathbf{q}'} \rangle + \langle \zeta_{\mathbf{k}-\mathbf{p}} \zeta_{\mathbf{k}'-\mathbf{p}'} \rangle \langle \zeta_{\mathbf{p}-\mathbf{q}} \zeta_{\mathbf{q}'} \rangle \langle \zeta_{\mathbf{q}} \zeta_{\mathbf{p}'-\mathbf{q}'} \rangle \\
&+ \langle \zeta_{\mathbf{k}-\mathbf{p}} \zeta_{\mathbf{p}'-\mathbf{q}'} \rangle \langle \zeta_{\mathbf{p}-\mathbf{q}} \zeta_{\mathbf{k}'-\mathbf{p}'} \rangle \langle \zeta_{\mathbf{q}} \zeta_{\mathbf{q}'} \rangle + \langle \zeta_{\mathbf{k}-\mathbf{p}} \zeta_{\mathbf{p}'-\mathbf{q}'} \rangle \langle \zeta_{\mathbf{p}-\mathbf{q}} \zeta_{\mathbf{q}'} \rangle \langle \zeta_{\mathbf{q}} \zeta_{\mathbf{k}'-\mathbf{p}'} \rangle \\
&+ \langle \zeta_{\mathbf{k}-\mathbf{p}} \zeta_{\mathbf{q}'} \rangle \langle \zeta_{\mathbf{p}-\mathbf{q}} \zeta_{\mathbf{k}'-\mathbf{p}'} \rangle \langle \zeta_{\mathbf{q}} \zeta_{\mathbf{p}'-\mathbf{q}'} \rangle + \langle \zeta_{\mathbf{k}-\mathbf{p}} \zeta_{\mathbf{q}'} \rangle \langle \zeta_{\mathbf{p}-\mathbf{q}} \zeta_{\mathbf{p}'-\mathbf{q}'} \rangle \langle \zeta_{\mathbf{q}} \zeta_{\mathbf{k}'-\mathbf{p}'} \rangle \\
&= \frac{(2\pi^2)^3}{(k-p)^3 (p-q)^3 q^3} \delta(\mathbf{k}+\mathbf{k}') \delta(\mathbf{p}+\mathbf{p}') \delta(\mathbf{q}+\mathbf{q}') P_\zeta(k-p) P_\zeta(p-q) P_\zeta(q) \\
&+ \frac{(2\pi^2)^3}{(k-p)^3 (p-q)^3 q^3} \delta(\mathbf{k}+\mathbf{k}') \delta(\mathbf{p}+\mathbf{p}') \delta(\mathbf{q}+\mathbf{p}'-\mathbf{q}') P_\zeta(k-p) P_\zeta(p-q) P_\zeta(q) \\
&+ \frac{(2\pi^2)^3}{(k-p)^3 (p-q)^3 q^3} \delta(\mathbf{k}+\mathbf{k}') \delta(\mathbf{p}-\mathbf{q}-\mathbf{k}-\mathbf{p}') \delta(\mathbf{q}+\mathbf{q}') P_\zeta(k-p) P_\zeta(p-q) P_\zeta(q) \\
&+ \frac{(2\pi^2)^3}{(k-p)^3 (p-q)^3 q^3} \delta(\mathbf{k}+\mathbf{k}') \delta(\mathbf{p}-\mathbf{q}+\mathbf{q}') \delta(\mathbf{q}-\mathbf{k}-\mathbf{p}') P_\zeta(k-p) P_\zeta(p-q) P_\zeta(q) \\
&+ \frac{(2\pi^2)^3}{(k-p)^3 (p-q)^3 q^3} \delta(\mathbf{k}+\mathbf{k}') \delta(\mathbf{p}-\mathbf{k}-\mathbf{q}') \delta(\mathbf{q}+\mathbf{p}'-\mathbf{q}') P_\zeta(k-p) P_\zeta(p-q) P_\zeta(q) \\
&+ \frac{(2\pi^2)^3}{(k-p)^3 (p-q)^3 q^3} \delta(\mathbf{k}+\mathbf{k}') \delta(-\mathbf{k}+\mathbf{p}-\mathbf{q}') \delta(\mathbf{q}-\mathbf{k}-\mathbf{p}') P_\zeta(k-p) P_\zeta(p-q) P_\zeta(q) .
\end{aligned} \tag{B.1}$$

## C Two-loop diagrams of third order SIGWs

The two-loop diagrams of of third order SIGWs are shown in following figures.

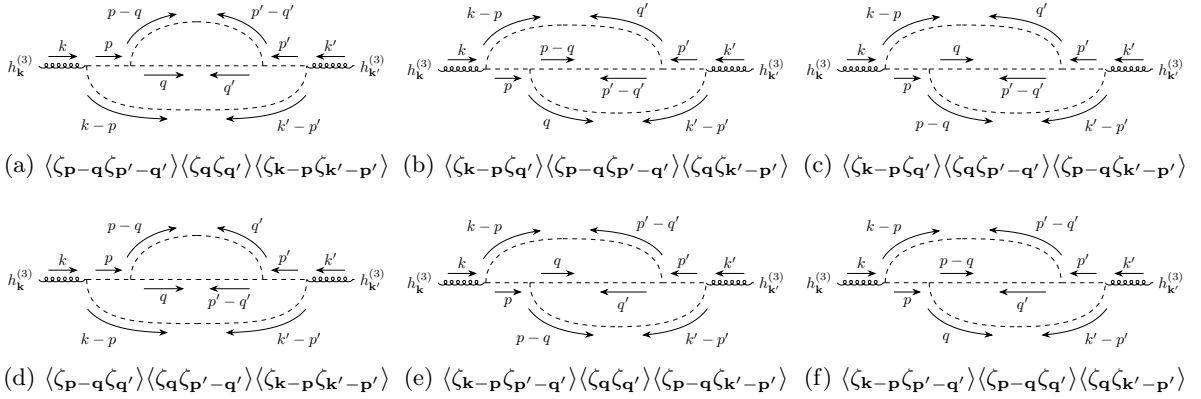


**Figure 9:** The two-point function  $\langle h_{\mathbf{k},\phi\psi\phi\phi}^{\lambda,(3)} h_{\mathbf{k}',\phi\psi\phi\phi}^{\lambda',(3)} \rangle$ . The diagrams correspond to the Wick's expansions of six-point correlation function. The dashed lines, wavy lines and spring-like lines represent scalar, vector, and tensor perturbations, respectively.

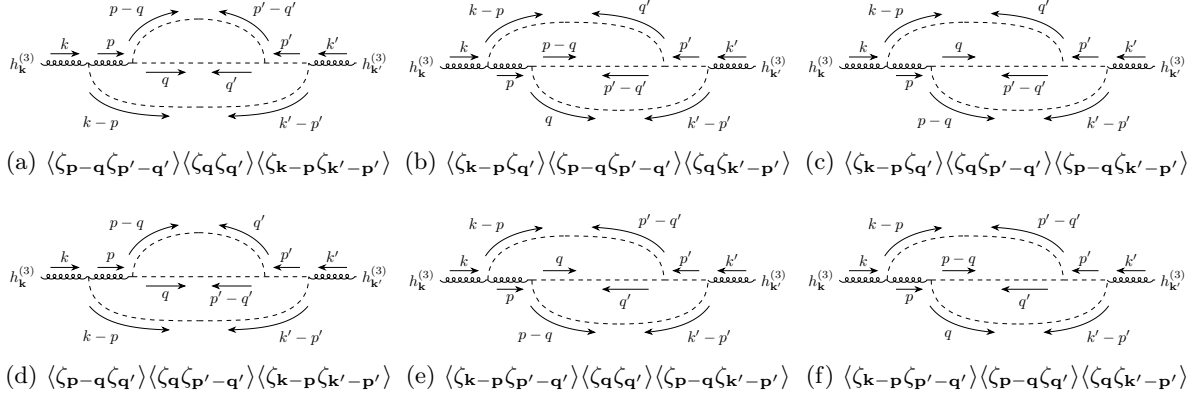


Figure 10: The two-point function  $\langle h_{\mathbf{k},\phi}^{\lambda,(3)} h_{\mathbf{k}',\phi\psi}^{\lambda',(3)} \rangle$ .

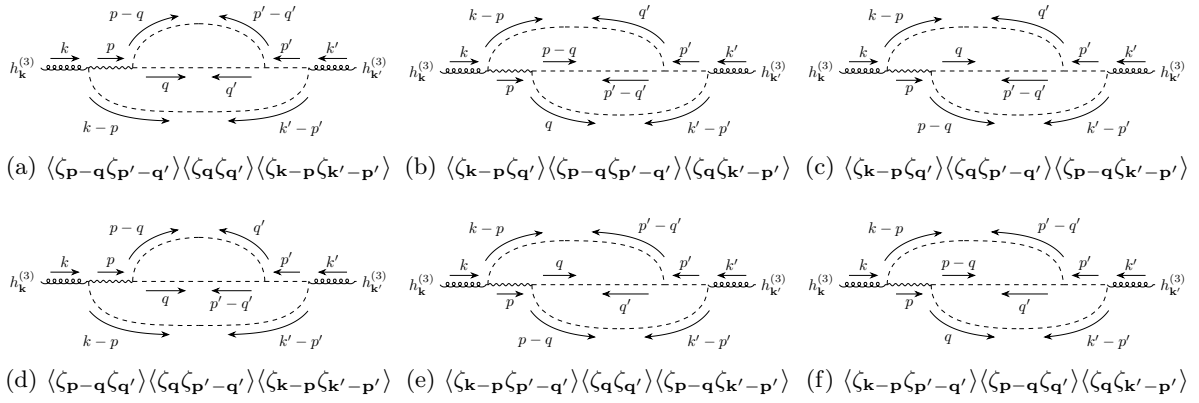


Figure 11: The two-point function  $\langle h_{\mathbf{k},\phi V_{\phi\phi}}^{\lambda,(3)} h_{\mathbf{k}',\phi\psi}^{\lambda',(3)} \rangle$ .

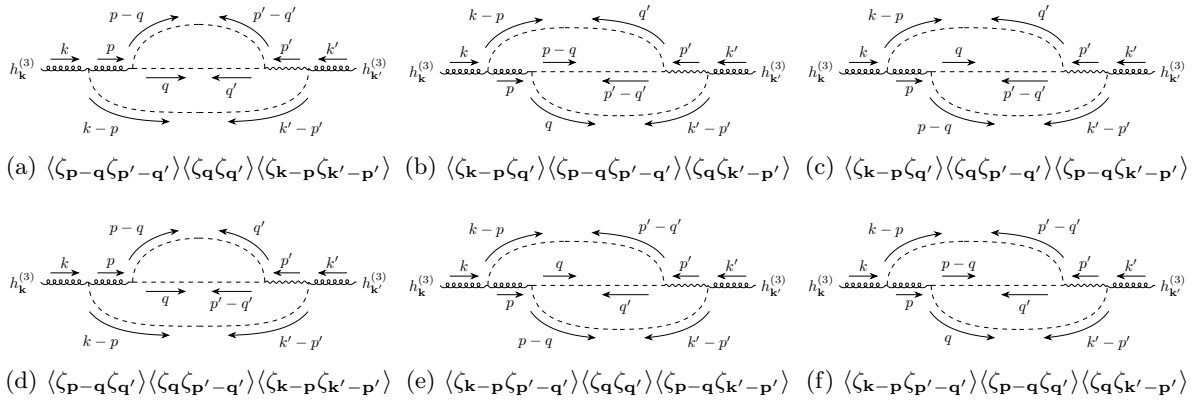


Figure 12: The two-point function  $\langle h_{\mathbf{k},\phi h_{\phi\phi}}^{\lambda,(3)} h_{\mathbf{k}',\phi V_{\phi\phi}}^{\lambda',(3)} \rangle$ .





## References

- [1] M. Hindmarsh, S.J. Huber, K. Rummukainen and D.J. Weir, *Shape of the acoustic gravitational wave power spectrum from a first order phase transition*, *Phys. Rev. D* **96** (2017) 103520 [[1704.05871](#)].
- [2] H.-K. Guo, K. Sinha, D. Vagie and G. White, *Phase Transitions in an Expanding Universe: Stochastic Gravitational Waves in Standard and Non-Standard Histories*, *JCAP* **01** (2021) 001 [[2007.08537](#)].
- [3] T. Hiramatsu, M. Kawasaki and K. Saikawa, *Gravitational Waves from Collapsing Domain Walls*, *JCAP* **05** (2010) 032 [[1002.1555](#)].
- [4] J.J. Blanco-Pillado, K.D. Olum and B. Shlaer, *Large parallel cosmic string simulations: New results on loop production*, *Phys. Rev. D* **83** (2011) 083514 [[1101.5173](#)].
- [5] M. Kawasaki and K. Saikawa, *Study of gravitational radiation from cosmic domain walls*, *JCAP* **09** (2011) 008 [[1102.5628](#)].
- [6] M. Rajagopal and R.W. Romani, *Ultralow frequency gravitational radiation from massive black hole binaries*, *Astrophys. J.* **446** (1995) 543 [[astro-ph/9412038](#)].
- [7] B. Kocsis and A. Sesana, *Gas driven massive black hole binaries: signatures in the nHz gravitational wave background*, *Mon. Not. Roy. Astron. Soc.* **411** (2011) 1467 [[1002.0584](#)].
- [8] K.N. Ananda, C. Clarkson and D. Wands, *Cosmological gravitational wave background from primordial density perturbations*, *Physical Review D* **75** (2007) .
- [9] K. Kohri and T. Terada, *Semianalytic calculation of gravitational wave spectrum nonlinearly induced from primordial curvature perturbations*, *Phys. Rev. D* **97** (2018) 123532 [[1804.08577](#)].
- [10] NANOGrav collaboration, *The NANOGrav 15 yr Data Set: Evidence for a Gravitational-wave Background*, *Astrophys. J. Lett.* **951** (2023) L8 [[2306.16213](#)].
- [11] NANOGrav collaboration, *The NANOGrav 15 yr Data Set: Observations and Timing of 68 Millisecond Pulsars*, *Astrophys. J. Lett.* **951** (2023) L9 [[2306.16217](#)].
- [12] NANOGrav collaboration, *The NANOGrav 15 yr Data Set: Search for Signals from New Physics*, *Astrophys. J. Lett.* **951** (2023) L11 [[2306.16219](#)].
- [13] EPTA collaboration, *The second data release from the European Pulsar Timing Array I. The dataset and timing analysis*, [2306.16224](#).
- [14] J. Antoniadis, P. Arumugam, S. Arumugam, S. Babak, M. Bagchi, A.S.B. Nielsen et al., *The second data release from the european pulsar timing array ii. customised pulsar noise models for spatially correlated gravitational waves*, 2023.
- [15] J. Antoniadis, P. Arumugam, S. Arumugam, S. Babak, M. Bagchi, A.S.B. Nielsen et al., *The second data release from the european pulsar timing array iii. search for gravitational wave signals*, 2023.
- [16] J. Antoniadis, P. Arumugam, S. Arumugam, S. Babak, M. Bagchi, A.S.B. Nielsen et al., *The second data release from the european pulsar timing array iv. search for continuous gravitational wave signals*, 2023.
- [17] J. Antoniadis, P. Arumugam, S. Arumugam, P. Auclair, S. Babak, M. Bagchi et al., *The second data release from the european pulsar timing array: V. implications for massive black holes, dark matter and the early universe*, 2023.
- [18] C. Smarra, B. Goncharov, E. Barausse, J. Antoniadis, S. Babak, A.S.B. Nielsen et al., *The second data release from the european pulsar timing array: Vi. challenging the ultralight dark matter paradigm*, 2023.
- [19] D.J. Reardon, A. Zic, R.M. Shannon, G.B. Hobbs, M. Bailes, V.D. Marco et al., *Search for an isotropic gravitational-wave background with the parkes pulsar timing array*, *The Astrophysical Journal Letters* **951** (2023) L6.
- [20] D.J. Reardon, A. Zic, R.M. Shannon, V.D. Marco, G.B. Hobbs, A. Kapur et al., *The gravitational-wave background null hypothesis: Characterizing noise in millisecond pulsar arrival times with the parkes pulsar timing array*, *The Astrophysical Journal Letters* **951** (2023) L7.

- [21] A. Zic, D.J. Reardon, A. Kapur, G. Hobbs, R. Mandow, M. Curyło et al., *The parkes pulsar timing array third data release*, 2023.
- [22] H. Xu et al., *Searching for the Nano-Hertz Stochastic Gravitational Wave Background with the Chinese Pulsar Timing Array Data Release I*, *Res. Astron. Astrophys.* **23** (2023) 075024 [2306.16216].
- [23] J. Ellis, M. Lewicki, C. Lin and V. Vaskonen, *Cosmic Superstrings Revisited in Light of NANOGrav 15-Year Data*, 2306.17147.
- [24] N. Kitajima, J. Lee, K. Murai, F. Takahashi and W. Yin, *Nanohertz Gravitational Waves from Axion Domain Walls Coupled to QCD*, 2306.17146.
- [25] Y. Bai, T.-K. Chen and M. Korwar, *QCD-Collapsed Domain Walls: QCD Phase Transition and Gravitational Wave Spectroscopy*, 2306.17160.
- [26] K. Fujikura, S. Girmohanta, Y. Nakai and M. Suzuki, *NANOGrav Signal from a Dark Conformal Phase Transition*, 2306.17086.
- [27] T. Bringmann, P.F. Depta, T. Konstandin, K. Schmidt-Hoberg and C. Tasillo, *Does NANOGrav observe a dark sector phase transition?*, 2306.09411.
- [28] P.F. Depta, K. Schmidt-Hoberg, P. Schwaller and C. Tasillo, *Do pulsar timing arrays observe merging primordial black holes?*, 2306.17836.
- [29] S. Balaji, G. Domènech and G. Franciolini, *Scalar-induced gravitational wave interpretation of PTA data: the role of scalar fluctuation propagation speed*, 2307.08552.
- [30] Y.-F. Cai, X.-C. He, X. Ma, S.-F. Yan and G.-W. Yuan, *Limits on scalar-induced gravitational waves from the stochastic background by pulsar timing array observations*, 2306.17822.
- [31] S. Wang, Z.-C. Zhao, J.-P. Li and Q.-H. Zhu, *Exploring the implications of 2023 pulsar timing array datasets for scalar-induced gravitational waves and primordial black holes*, 2023.
- [32] S. Vagnozzi, *Inflationary interpretation of the stochastic gravitational wave background signal detected by pulsar timing array experiments*, *JHEAp* **39** (2023) 81 [2306.16912].
- [33] K. Inomata, K. Kohri and T. Terada, *The Detected Stochastic Gravitational Waves and Subsolar-Mass Primordial Black Holes*, 2306.17834.
- [34] S. Saga, *The Vector Mode in the Second-order Cosmological Perturbation Theory*, Ph.D. thesis, Nagoya U. (main), 2017. 10.1007/978-981-10-8007-4.
- [35] PLANCK collaboration, *Planck 2018 results. X. Constraints on inflation*, *Astron. Astrophys.* **641** (2020) A10 [1807.06211].
- [36] P. Adshead, K.D. Lozanov and Z.J. Weiner, *Non-Gaussianity and the induced gravitational wave background*, *JCAP* **10** (2021) 080 [2105.01659].
- [37] C. Yuan, D.-S. Meng and Q.-G. Huang, *Full analysis of the scalar-induced gravitational waves for the curvature perturbation with local-type non-Gaussianities*, 2308.07155.
- [38] J.-P. Li, S. Wang, Z.-C. Zhao and K. Kohri, *Complete Analysis of Scalar-Induced Gravitational Waves and Primordial Non-Gaussianities  $f_{\text{NL}}$  and  $g_{\text{NL}}$* , 2309.07792.
- [39] C. Yuan and Q.-G. Huang, *A topic review on probing primordial black hole dark matter with scalar induced gravitational waves*, *iScience* **24** (2021) 102860 [2103.04739].
- [40] V. De Luca, A. Kehagias and A. Riotto, *How well do we know the primordial black hole abundance: The crucial role of nonlinearities when approaching the horizon*, *Phys. Rev. D* **108** (2023) 063531 [2307.13633].
- [41] J.-C. Hwang, D. Jeong and H. Noh, *Gauge dependence of gravitational waves generated from scalar perturbations*, *Astrophys. J.* **842** (2017) 46 [1704.03500].
- [42] C. Yuan, Z.-C. Chen and Q.-G. Huang, *Scalar induced gravitational waves in different gauges*, *Phys. Rev. D* **101** (2020) 063018 [1912.00885].
- [43] K. Inomata and T. Terada, *Gauge Independence of Induced Gravitational Waves*, *Phys. Rev. D* **101** (2020) 023523 [1912.00785].

- [44] G. Domènech, S. Passaglia and S. Renaux-Petel, *Gravitational waves from dark matter isocurvature*, *JCAP* **03** (2022) 023 [2112.10163].
- [45] S. Saga, K. Ichiki and N. Sugiyama, *Impact of anisotropic stress of free-streaming particles on gravitational waves induced by cosmological density perturbations*, *Phys. Rev. D* **91** (2015) 024030 [1412.1081].
- [46] X. Zhang, J.-Z. Zhou and Z. Chang, *Impact of the free-streaming neutrinos to the second order induced gravitational waves*, *Eur. Phys. J. C* **82** (2022) 781 [2208.12948].
- [47] C. Yuan, Z.-C. Chen and Q.-G. Huang, *Probing primordial–black-hole dark matter with scalar induced gravitational waves*, *Phys. Rev. D* **100** (2019) 081301 [1906.11549].
- [48] J.-Z. Zhou, X. Zhang, Q.-H. Zhu and Z. Chang, *The third order scalar induced gravitational waves*, *JCAP* **05** (2022) 013 [2106.01641].
- [49] Z. Chang, Y.-T. Kuang, X. Zhang and J.-Z. Zhou, *Primordial black holes and third order scalar induced gravitational waves\**, *Chin. Phys. C* **47** (2023) 055104 [2209.12404].
- [50] S. Wang, Z.-C. Zhao and Q.-H. Zhu, *Constraints On Scalar-Induced Gravitational Waves Up To Third Order From Joint Analysis of BBN, CMB, And PTA Data*, 2307.03095.
- [51] K. Inomata, *Analytic solutions of scalar perturbations induced by scalar perturbations*, *JCAP* **03** (2021) 013 [2008.12300].
- [52] Z. Chang, X. Zhang and J.-Z. Zhou, *The cosmological vector modes from a monochromatic primordial power spectrum*, *JCAP* **10** (2022) 084 [2207.01231].
- [53] Z. Chang, S. Wang and Q.-H. Zhu, *Note on gauge invariance of second order cosmological perturbations*, *Chin. Phys. C* **45** (2021) 095101 [2009.11025].
- [54] S. Wang, T. Terada and K. Kohri, *Prospective constraints on the primordial black hole abundance from the stochastic gravitational-wave backgrounds produced by coalescing events and curvature perturbations*, *Phys. Rev. D* **99** (2019) 103531 [1903.05924].
- [55] PLANCK collaboration, *Planck 2018 results. VI. Cosmological parameters*, *Astron. Astrophys.* **641** (2020) A6 [1807.06209].
- [56] K. Saikawa and S. Shirai, *Primordial gravitational waves, precisely: The role of thermodynamics in the Standard Model*, *JCAP* **05** (2018) 035 [1803.01038].
- [57] G.P. Lepage, *A New Algorithm for Adaptive Multidimensional Integration*, *J. Comput. Phys.* **27** (1978) 192.
- [58] G.P. Lepage, *Adaptive multidimensional integration: VEGAS enhanced*, *J. Comput. Phys.* **439** (2021) 110386 [2009.05112].
- [59] P. Lepage, *gplepage/vegas: vegas version 5.6*, Dec., 2023. 10.5281/zenodo.10402580.
- [60] X. Siemens, J. Ellis, F. Jenet and J.D. Romano, *The stochastic background: scaling laws and time to detection for pulsar timing arrays*, *Class. Quant. Grav.* **30** (2013) 224015 [1305.3196].
- [61] T. Robson, N.J. Cornish and C. Liu, *The construction and use of LISA sensitivity curves*, *Class. Quant. Grav.* **36** (2019) 105011 [1803.01944].
- [62] Z.-C. Zhao and S. Wang, *Bayesian Implications for the Primordial Black Holes from NANOGrav’s Pulsar-Timing Data Using the Scalar-Induced Gravitational Waves*, *Universe* **9** (2023) 157 [2211.09450].
- [63] W.G. Lamb, S.R. Taylor and R. van Haasteren, *Rapid refitting techniques for bayesian spectral characterization of the gravitational wave background using pulsar timing arrays*, *Physical Review D* **108** (2023) 103019.
- [64] A. Mitridate, D. Wright, R. von Eckardstein, T. Schröder, J. Nay, K. Olum et al., *Ptarcade*, 2023.
- [65] M.A. Gorji, M. Sasaki and T. Suyama, *Extra-tensor-induced origin for the PTA signal: No primordial black hole production*, *Phys. Lett. B* **846** (2023) 138214 [2307.13109].
- [66] Z. Chang, X. Zhang and J.-Z. Zhou, *Gravitational waves from primordial scalar and tensor perturbations*, *Phys. Rev. D* **107** (2023) 063510 [2209.07693].

- [67] C. Chen, A. Ota, H.-Y. Zhu and Y. Zhu, *Missing one-loop contributions in secondary gravitational waves*, *Phys. Rev. D* **107** (2023) 083518 [[2210.17176](#)].